AD-A081 235 CASE WESTERN RESERVE UNIV CLEVELAND OH CASE LABS FOR--ETC F/G 7/4
A MECHANISTIC STUDY OF O2 REDUCTION ON WATER SOLUBLE PHTHALOCYA--ETC(U)
OCT 79 J ZAGAL, P BINDRA, E YEAGER N00014-75-C-0953
UNCLASSIFIED TR-50 NL

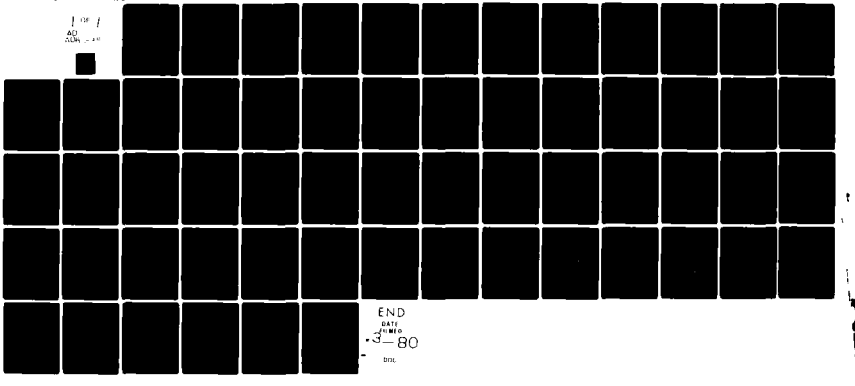

END
DATE FILMED
3-80
DTIC

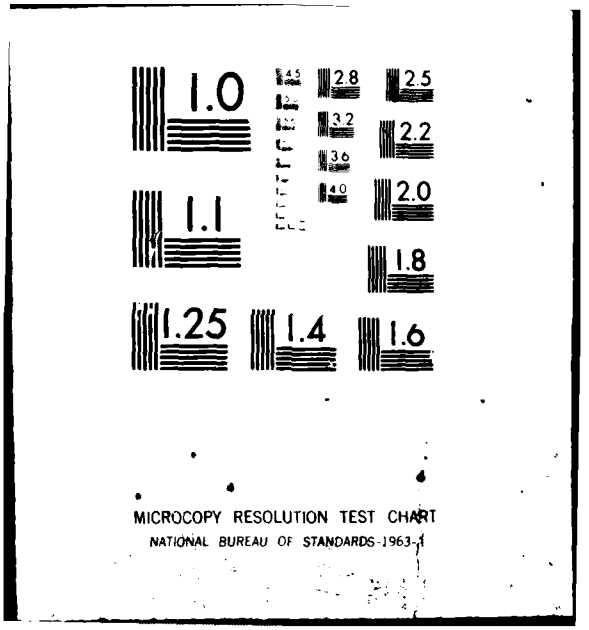
1.0
1.1
1.25
1.4
1.6
1.8
2.0
2.2
2.5
2.8
3.2
3.6
4.0
4.5
MICROCOPY RESOLUTION TEST CHART
NATIONAL BUREAU OF STANDARDS-1963-A

OFFICE OF NAVAL RESEARCH

Contract N00014-75C-0953

Task No. NR 359-451

Technical Report No. 58

A Mechanistic Study of O_2 Reduction on Water Soluble Phthalocyanines Adsorbed on Graphite Electrodes.

by

J. Zagal, P. Bindra and E. Yeager

Case Laboratories for Electrochemical Studies,
and the Chemistry Department
Case Western Reserve University
Cleveland, Ohio 44106

Prepared for submission

to the

Journal of the Electrochemical Society

October 1, 1979

58

REPORT DOCUMENTATION PAGE		READ INSTRUCTIONS BEFORE COMPLETING FORM
1. REPORT NUMBER 50	2. GOVT ACCESSION NO.	3. RECIPIENT'S CATALOG NUMBER
4. TITLE (and Subtitle) A Mechanistic Study of O_2 Reduction on Water Soluble Phthalocyanines Adsorbed on Graphite Electrodes		5. TYPE OF REPORT & PERIOD COVERED Technical Report #50
		6. PERFORMING ORG. REPORT NUMBER
7. AUTHOR(s) J. Zagal, P. Bindra and E. Yeager		8. CONTRACT OR GRANT NUMBER(s) N00014-75C-0953
9. PERFORMING ORGANIZATION NAME AND ADDRESS Dept. of Chemistry Case Western Reserve University Cleveland, Ohio 44106		10. PROGRAM ELEMENT, PROJECT, TASK AREA & WORK UNIT NUMBERS NR 359-451
11. CONTROLLING OFFICE NAME AND ADDRESS Office of Naval Research Chemistry Program - Chemistry Code 472 Arlington, Virginia 22217		12. REPORT DATE 1 Oct 1979
		13. NUMBER OF PAGES 52
14. MONITORING AGENCY NAME & ADDRESS (if different from Controlling Office)		15. SECURITY CLASS. (of this report) Unclassified
		15a. DECLASSIFICATION/DOWNGRADING SCHEDULE
16. DISTRIBUTION STATEMENT (of this Report) This document has been approved for public release and sale; its distribution unlimited.		
17. DISTRIBUTION STATEMENT (of the abstract entered in Block 20, if different from Report)		
18. SUPPLEMENTARY NOTES		
19. KEY WORDS (Continue on reverse side if necessary and identify by block number) oxygen electrode, transition metal macrocyclics, oxygen electrocatalysis, phthalocyanines		
20. ABSTRACT (Continue on reverse side if necessary and identify by block number) Co and Fe tetrasulfonate phthalocyanines (M-TSP), adsorbed at monolayer levels on graphite surfaces, have been found to have a pronounced catalytic effect on the O_2 reduction process in both acid and alkaline solutions. The kinetics have been examined with the rotating ring-disk electrode technique. Co-TSP promotes the O_2 reduction process via 2-electrons to give peroxide whereas Fe-TSP promotes a 4-electron reduction to give water.		

DD FORM 1 JAN 73 1473 EDITION OF 1 NOV 65 IS OBSOLETE
S/N 0102-LF-014-6601

Unclassified
SECURITY CLASSIFICATION OF THIS PAGE (When Data Entered)

TABLE OF CONTENTS

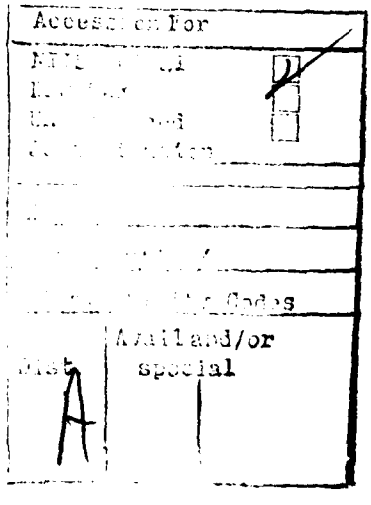

List of Figures - Shown consecutively beginning on page 30.

A Mechanistic Study of O_2 Reduction on Water Soluble Phthalocyanines Adsorbed on Graphite Electrodes

J. Zagal,* P. Bindra and E. Yeager

Case Laboratories for Electrochemical Studies
and the Chemistry Department
Case Western Reserve University
Cleveland, Ohio 44106

Abstract

Co and Fe tetrasulfonate phthalocyanines (M-TSP), adsorbed at monolayer levels on graphite surfaces, have been found to have a pronounced catalytic effect on the O_2 reduction process in both acid and alkaline solutions. The kinetics have been examined with the rotating ring-disk electrode technique. Co-TSP promotes the O_2 reduction process via 2-electrons to give peroxide whereas Fe-TSP promotes a 4-electron reduction to give water.

*On leave of absence from Universidad Tecnica del Estado, Santiago, Chile.

Key Words: Oxygen electrode, transition metal macrocyclics, oxygen electrocatalysis, phthalocyanines.

I. Introduction

The catalytic properties of metal phthalocyanines for the electroreduction of O_2 have been examined extensively in the literature (see e.g. 1 -10, 40). In general, macrocyclic transition metal complexes of this type have been found to have catalytic activity for the O_2 reduction process. A comprehensive review on this field has been published recently (1). Basic kinetic and mechanistic studies of the process, however, are less available. A direct correlation has been found (2-4) between the first oxidation potential of the metal phthalocyanine and its catalytic activity for O_2 reduction. Beck (4) has recently proposed a mechanism for the process based on data for O_2 reduction on Co tetraazaannulene (Co-TAA), which gives Tafel slopes of -60mV/decade in acid solution. This author proposed that the metal complex reacts with oxygen according to the reaction:

$$M^{II} + O_2 \xrightarrow{H^+} M^{III} - O_2H \qquad (a)$$

where O_2 undergoes partial reduction with simultaneous oxidation of the metal center. The O_2 adduct, according to Beck, then undergoes a 2-electron reduction as the rate determining step, regenerating the catalyst. For a transfer coefficient $\alpha = 0.5$, the Tafel slope could then be -60mV/decade. Simultaneous 2-electron steps, however, are unlikely on energetic grounds.

A mechanism has been recently proposed by Appleby and Savy (5, 8) based on studies of O_2 reduction on Fe phthalocyanines. According to these authors, the rate determining step is the breaking of the O-O bond

and the proposed mechanism in basic media is:

$$O_2 \rightleftharpoons O_{2_{ads}} \qquad (b)$$

$$O_{2_{ads}} + H_2O + e^- \rightleftharpoons O_2H_{ads} + OH^- \qquad (c)$$

$$O_2H_{ads} + e^- \rightleftharpoons O_2H^-_{ads} \qquad (d)$$

$$O_2H^-_{ads} + H_2O \longrightarrow 2\ OH^-_{ads} + OH^-. \qquad (e)$$

Even though this mechanism explains the experimental data, it does not explain the specific involvement of the catalyst and particularly the valency state of the transition metal in the reaction sequence. Further, it is unlikely that the superoxide species $(O_2H)_{ads}$ is protonated in alkaline electrolytes in view of the ionization constant(pK = 4.88) for the O_2H species in solution (41).

The present work has involved the catalytic properties of water soluble tetrasulfonated phthalocyanine s adsorbed on graphite substrates. As previously reported (9,11), considerable catalytic activity can be achieved by adsorbing these complexes from aqueous solutions. The redox properties of the catalysts can be determined using cyclic voltammetry under the same conditions (pH, solvent) at which the O_2 reduction experiments are carried out. This type of approach is facilitated by use of the basal plane of stress-annealed pyrolytic graphite (SAPG) with x-ray diffraction rocking angles as small as $\Delta\theta_{1/2} = 0.4°$. This material provides a near ideal surface for studying the redox properties of adsorbed species because of its low background currents (22) and very low catalytic activity for the O_2 reduction process (23).

II. Experimental Procedure

A disk electrode, exposing the basal plane of SAPG (9-23) with an area of 0.20 cm^2, was used for most of the rotating disk measurements. For the ring-disk electrode measurements, the disk was constructed with ordinary pyrolytic graphite (OPG) (radius = 0.250 cm) with gold (99.99% pure) as the ring (inner radius - 0.272 cm, outer radius = 0.357 cm). The OPG had an x-ray rocking angle of $\Delta\theta_{1/2} = 45°$. Unfortunately the fragile nature of the SAPG prevented its use as the disk in the ring-disk experiments. Unless otherwise indicated, all measurements on SAPG and OPG were on the basal plane.

The ring-disk electrode was calibrated with the ferrous/ferric couple using 10^{-2} and 10^{-3} M $Fe_2(SO_4)_3$ in 0.05M H_2SO_4. The value of the collection efficienty[2] N determined in this manner was 0.382. This value compared favorably with the calculated value of 0.38 obtained from the geometry of the electrodes using the tables of Albery and Bruckenstein (12). The Teflon cell had separate compartments for the reference (saturated calomel-SCE) and counter electrode (Au-foil) with an additional isolation compartment between the working and reference compartments. A Teflon Luggin capillary was used to minimize IR drop with its tip ∿3mm below the center of the rotating disk electrode. The polarization curves for the kinetic measurements were obtained by starting at the open-circuit potential and scanning toward more negative values at a rate of 10 mV/s. The hysteresis on reverse of sweep was negligible at these scan rates. Small currents (i.e., < 10μA) were measured point by point by waiting at each potential for the drift rate to become negligible. All measurements were made at 20 to 22°C.

---

[1] The SAPG and OPG were provided by the Union Carbide Corporation through Dr. A. Moore of the Parma Technical Research Center, Parma, Ohio.

[2] $N = I_R / I_D$ where I_R is the ring current and I_D is the disk current.

The surface of the basal plane of SAPG was renewed by use of the adhesive tape technique with care to avoid contamination of the Teflon mounting with the adhesive of the tape (9,21,23). The OPG electrodes were polished using 0.3 μ alumina suspended in water with water on microcloth for the final polish. The M-TSP was adsorbed on the graphite surface by placing a drop of solution of the complex (10^{-5}M) on the electrode. Similar results were obtained when the adsorbed layer was applied by submerging the electrode in a 10^{-5}M solution of the complex. The electrode was subsequently washed with purified water (pyrolyzed over Pt/Rh at 800°C). For experiments in acid solution some of this complex was added to the electrolyte to preserve the adsorbed catalyst layer during the measurements. In the other electrolytic solutions the adsorption was sufficiently strong to render the loss of the adsorbed complex negligible over the duration of the measurements.

Basic (0.1M NaOH) and acid (0.05M H_2SO_4) solutions were prepared as described before (9). Other solutions of various pH were as follows: 1M NaOH: pH - 13.8; 0.1M NaOH: pH = 12.9; 0.1M Na_2CO_3: pH - 11.5; 0.005M Na_2CO_3 + 0.05M Na_2SO_4: pH = 10.8; 0.0015M NaOH + 0.05M H_3BO_3 + 0.05M Na_2SO_4: pH - 8.7; 0.10M NaOH + 0.05M H_3BO_3 + 0.05M Na_2SO_4: pH = 6.3 and 0.1M NaH_2PO_4 : pH = 4.4. Special precautions were taken to minimize $CO_3^=$ in the alkaline electrolytes. The Co-TSP and Fe-TSP were prepared and purified by the procedures described by Weber and Busch (38).

III. Results

A. Cyclic Voltammetry Measurements

Figure 1 shows the cyclic voltammetry curves obtained at different potential scan rates for Co-TSP pre-adsorbed on the basal plane of SAPG. A Teflon hood, similar to that described by Randin and Yeager (39) was used

to eliminate edge effects and leakage of the electrolyte between the Teflon and the side of the disk electrode, which otherwise cause a pronounced slant in the voltammetry curves. The peak currents are directly proportional to the scan rate, which is typical of a Faradaic process involving an adsorbed species. (For the adsorption of a diffusing species the peak currents are directly proportional to the square root of the scan rate.)

From the area under the peak, the charge involved in the process can be estimated. An experimental value of 3 $\mu C/cm^2$ has been determined, which corresponds to a surface concentration of 3×10^{-11} moles/cm^2 of adsorbed metal complex assuming that a one-electron transfer process is involved. Assuming that the surface redox couple obeys the Nernst equation, the peak current for the voltammetry is given by:

$$i_p = \frac{n^2 F \Gamma \nu}{4 RT} \qquad (1)$$

where Γ is the total surface concentration of the adsorbed complex in moles/cm^2, ν is the potential scan rate and n is the number of electrons per adsorbed molecule. The charge under the peak is known and is equal to $Q = nF\Gamma$. Experimental values of Q and i_p give n = 0.9 or $\sim$ 1, indicating that one electron is involved in the surface redox process, which is likely to involve the metal center (13-14); i.e.,

$$(Co^{II}TSP)_{ads} \rightleftharpoons (Co^{III}TSP)_{ads} + e^- \qquad (f)$$

The small deviation of n from unity is probably caused by the approximate nature of eq. 1, which assumes that the Nernst equation is followed with the activities for the adsorbed species in the two different valence states replaced by the surface concentrations.

Co-TSP readily adsorbs on other carbon substrates including glassy carbon, the edge-orientation of SAPG and ordinary pyrolytic graphite (OPG). Because of the high background currents of graphite surfaces other than the basal plane of SAPG, however, less well defined cyclic voltammetry curves result. For Co-TSP adsorbed on the basal plane of OPG, the charge estimated from cyclic voltammetry is ca. 13 $\mu C/cm^2$ which is about 4 times that found on the basal plane of SAPG.

The iron derivative also readily adsorbed on the basal plane of SAPG as evidenced by the voltammetry curve shown in Figure 2. From the scan rate dependence of both peaks 1 and 2, it was established that a one elcctron transfer is involved in each case. The charge under each peak estimated from the area between the solid and the dotted lines in Figure 2, is $\sim$3.0 $\mu C/cm^2$, which is the same as found for Co-TSP. This charge is independent of potential scan rate over the range investigated (50 to 1000 mV/s). Even though this value is only approximate, it suggests that the surface coverages by Co-TSP and Fe-TSP species are essentially the same. For Fe-TSP adsorbed on the basal plane of OPG, the charge under both peaks 1 and 2 is 13 $\mu C/cm^2$ each, which is the value found for Co-TSP adsorbed on the same graphite material.

The voltammograms obtained at various pH indicate that the potentials of peaks 1 and 2 shift with pH. Peak 1 appears to involve the process $Fe^{III} + e^- \longrightarrow Fe^{II}$. This process is pH dependent over a range of pH depending on pK_A of the M-TSP. The fact that macrocyclic complexes of transition metals in the oxidation state III undergo hydrolysis in water solutions is a well known phenomenon (see e.g., ref. 15 and 16). The redox reaction can be written as:

$$S - \left[Fe^{III}\right]OH + H_2O + e^- \rightleftharpoons S - \left[Fe^{II}\right]OH_2 + OH^- \qquad (g)$$

where S represents the graphite substrate.

The potential of the Fe^{III}/Fe^{II} redox couple, according to reaction g, should shift with pH as $\Delta E/\Delta pH = -0.059$ V/pH. Figure 3 shows a plot of peak potential (peak 1) versus pH. The slope of the linear region is -0.057 V/pH, suggesting that a process such as reaction g is involved.

The position of peak 2 shifts with pH only at low pH values. It is not clear what type of process is involved in this case. The voltammetry curves suggest that the process is reversible. Perhaps in the reduced form the transferred electron is delocalized in the π system of the macrocyclic ligand or alternatively the Fe is in the equivalent of the I valent state. Lever and Wilshire (17) have reported that iron (II) phthalocyanine ($Fe^{II}Pc$) can be electrochemically reduced in non-aqueous solvents to give $Fe^{I}Pc$ in which Fe has been shown to be five coordinated on the basis of its electron spin resonance spectrum.

B. O_2 Reduction on Graphite with Adsorbed Co-TSP

The O_2 reduction currents on graphite surfaces other than the basal plane of graphite alkaline solution are large even in the absence of adsorbed transition met macrocyclics. This makes the interpretation of the electrocatalytic properties of the Co-TSP adsorbed on these surfaces difficult. On all of these surfaces, the presence of the macrocyclic greatly increases the O_2 kinetic reduction current (i_k). The observed current-voltage curves are compared with and without the adsorbed Co-TSP in Figure 4. The relatively low apparent limiting current for the basal plane of ordinary pyrolytic graphite is the result of combined diffusion and kinetic control with a potential insensitive chemical step (23).

For a process which is first order in a diffusing reactant, the disk

current is related to the rotation rate f by the expression (28,32)

$$1/i = (1/i_k) + 1/(Bf^{1/2}) \quad (2)$$

where B is related to the diffusion limiting current by

$$i_L = Bf^{1/2} \quad (2a)$$

and is given by

$$B = 0.20\ (D_{O_2})^{2/3}\nu^{-1/6}nFA\ C_{O_2} \quad (2b)$$

where D_{O_2} and C_{O_2} are the diffusion coefficient and solubility of O_2, ν is the kinematic viscosity, f is the rotation rate in radians, A is the area, F is the Faraday and n is the number of electrons transferred per molecule of O_2 diffusing through the Nernst boundary layer. The plot in Figure 5 for Co-TSP/SAPG in 0.1M NaOH clearly follows eq. 2, thus confirming first order dependence of the kinetics on O_2. Similar behavior has been observed in 0.05M H_2SO_4. This linearity also provides evidence for reasonable uniformity of the current distribution on the disk even at potentials other than corresponding to the diffusion limiting value (see discussion in Ref. 29).

The B values evaluated from the slopes in these plots are 1.47×10^{-2}mA(rpm)$^{1/2}$, which compares well with the theoretical value of 1.42×10^{-2}mA (rpm)$^{1/2}$, calculated with eq. 2b for n = 2, using the following values for both 0.05 H_2SO_4 and 0.1M NaOH: $C_{O_2} = 1.38 \times 10^{-6}$ moles/cm^2 (24); the diffusion coefficient reported by Gubbins and Walker (25) at 25°C ($D_{O_2} = 1.90 \times 10^{-5}$ cm^2/s) corrected to 20°C ($D_{O_2} = 1.67 \times 10^{-5}$ cm^2/s), using the mean temperature coefficient estimated from the data of Davies, Horvath and Tobias (26) [$d\ell nD_{O_2}/dt = 2.4\%/°C$]; $\nu = 9.97 \times 10^{-3}$ cm^2/s, estimated from the viscosity of 1.002×10^{-2}g cm^{-1}s^{-1} and density ρ = 1.005g/cm^3 (27);and A = 0.196 cm^2. This agreement confirms that the O_2 reduction catalyzed by adsorbed Co-TSP is the 2 e$^-$ reduction to the peroxide as the main product.

Kinetic data for O_2 reduction in 0.05M H_2SO_4 with Co-TSP adsorbed on various substrates using the rotating disk technique are summarized in Figure 6. The kinetic current densities have been corrected for diffusion by multiplying by the factor $i_L/(i_L-i)$ where i_L is the diffusion limiting current density obtained directly from the i vs. E plots. The Tafel plots are essentially identical (-155 mV/decade) for all of the substrates except the basal plane of SAPG with a low rocking angle ($\Delta\theta_{1/2}$ = 0.4°) for which the slope is -135 mV/decade. The lower slope on this surface may reflect the semiconductor properties (22) which influence the potential distribution at the surface or differences in the ionic double layer for the SAPG basal plane compared to other carbon surfaces.

Figure 7 indicates the Tafel type plots for O_2 reduction on Co-TSP adsorbed on SAPG of $\Delta\theta_{1/2}$ - 0.4° using the correction factor (I/I_L-I) where I and I_L are the current and diffusion limiting current. This factor has been used rather than $[I_L/I_L-I]$ in order that the data for several rotation rates may be clearly represented. The slope is -120mV/decade at 25°C, corresponding to an apparent α = 0.5.

Rotating ring-disk data for Co-TSP adsorbed on OPG is shown in Figure 8 for 0.1M NaOH. The gold ring was maintained at a potential in the diffusion limiting current range for the oxidation of peroxide (0.10V vs. SCE). Difficulty was encountered in obtaining well defined diffusion limiting currents for peroxide oxidation on the Au ring in 0.05M H_2SO_4 and consequently ring-disk experiments are not reported for this electrolyte.

To analyze the rotating ring-disk electrode data (Figure 8), consider the following series-parallel reaction scheme for O_2 reduction (19):

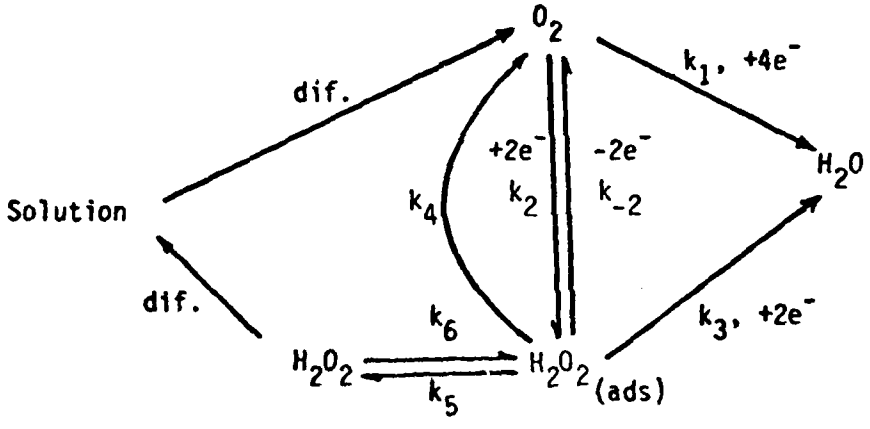

The disk-ring current ratio for the O_2 reduction process is as follows:

$$NI_D/I_R = 1 + (2k_1/k_2) + D + [k_6/(Z_{H_2O_2} f^{1/2}) X \quad (3)$$

where $X = (2k_1/k_2k_5)(k_{-2} + k_3 + k_4) + [(2k_3 + k_4)/k_5]$ (3a)

and $Z_{H_2O_2} = 0.62 D_{H_2O_2}^{2/3} \nu^{-1/6}$ (3b)

If we assume that adsorption equilibrium exists between H_2O_2 on the electrode surface and in the solution, eq. 3 becomes (18)

$$NI_D/I_R = 1 + (2k_1/k_2) + [1/(Z_{H_2O_2} f^{1/2})](2k_3' + k_4') + (2k_1/k_2)(k_{-2}' + k_3' + k_4') \quad (4)$$

where

$$k_{-2}' = K_{56}k_{-2};\ k_3' = K_{56}k_3;\ k_4' = K_{56}k_4 \quad (4a)$$

with $K_{56} = k_6/k_5$.

The diffusion limiting current for a 4-electron reduction of O_2 to yield OH^- or H_2O is given by

$$I_L' = 4\ AF\ Z_{O_2}\ C_{O_2}\ f^{1/2} \quad (5)$$

where

$$Z_{O_2} = 0.20\, D_{O_2}^{2/3}\, \nu^{-1/6} \qquad (5a)$$

It should be noted that I_L' is a theoretical value and not directly observed. Combining eq. 4 and 5 yields (18), we obtain

$$\frac{(I_L' - I_D)N}{I_R} = 1 + \frac{2\,(k_3' + k_4' + k'_{-2})}{k_2} \cdot \frac{Z_{O_2}}{Z_{H_2O_2}} + \frac{2Z_{O_2}}{k_2}\, f^{1/2} \qquad (6)$$

A plot of $(I_D/I_R)N$ vs. $f^{-1/2}$ is shown in Fig. 9. The scatter of the points is caused by the expansion of the ordinate, necessary as a result of the surprisingly low slope. This low slope and the closeness of the intercept to unity indicate that very little of the peroxide generated at the electrode is further reduced and that k_1 is small compared to k_2. Further analysis of the data can be done by plotting $(I'_L - I_D)N/I_R$ vs. $f^{1/2}$. This graph is shown in Fig. 10. The lines are straight as expected from eq. 6. From the slopes it is possible to evaluate k_2. The rate constant k_1 can be evaluated from the intercept in Fig. 9, using eq. 4. The scatter of the points in Fig. 9 is too great to permit the independently drawn straight lines through the data to be used to evaluate the intercepts. Consequently all of the lines in Fig. 9 have been drawn through the data with the same slopes. This assumption may not be fully justified and can influence the potential dependence of k_1.

The Tafel slopes evaluated from the E vs. log k plots (Fig. 11) are $dE/d \log k_1 = \sim -0.15$V/decade and $dE/d \log k_2 = \sim -0.12$V/decade, as compared with an apparent Tafel slope -0.12V/decade from the E vs. log $i/(i_L - i)$ plots (Fig. 7). The slope of the $dE/d \log k_1$ plot, however, is based on the assumption that the slopes in Fig. 9 are not potential dependent. In addition, the uncertainties in the intercepts in this figure are substantial even with this assumption. Most likely the potential dependence of k_1 is essentially the same as that of k_2.

C. O_2 Reduction on Adsorbed Fe-TSP

Figure 12 shows the polarization curves as solid lines obtained at different rotation rates on a ring-disk electrode with a pre-adsorbed layer of Fe-TSP on the

OPG disk. The same figure shows the O_2 reduction currents observed on this graphite material without Fe-TSP adsorbed on the surface. Also shown is the ring current measured at the diffusion limiting HO_2^- peroxide oxidation condition on the Au ring.

The ring currents at disk potentials more positive than -0.32V are zero, which indicates that the O_2 reduction occurs via 4-electrons with no detectable amount of peroxide at those potentials. The small amounts of HO_2^- detected at higher polarizations may be due in part to the O_2 reduction process on zones of the graphite uncovered by the Fe-TSP. The maximum in I_L for the OPG substrate occurs almost at the same potential as that for the Fe-TSP/OPG. On the other hand the maximum in I_L for the latter is far too pronounced to be caused just by I_L for the substrate. This maximum in I_L for Fe-TSP/graphite correlates well with the second peak in the voltammetry curve (see Figure 2).

Plots of $1/I$ vs. $1/f^{1/2}$ (Figure 13) yield parallel straight lines at potentials anodic to the maximum in Figure 13 as expected for a first order process on O_2. The currents at -0.6V correspond to pure diffusion control for the 4 e^- reduction, based on the intercept and slope in Figure 14 [B(exp) = 2.4×10^{-2} mA $rpm^{-1/2}$ as compared with B(theor) = 2.8×10^{-2} mA $rpm^{-1/2}$ for n = 4]. The deviation of the points at higher rotation rates and more anodic potentials on Fe-TSP/OPG is not fully explained but may be related to a change in rate controlling step in this potential region as discussed later.

Plots of $1/I$ vs. $1/f^{1/2}$ for potentials cathodic to -0.6V (Figure 14) have slopes which increase with potential; i.e., B decreases indicating that the 4 e^- process tends to revert to a 2 e^- process. This correlates well with the sharp increase in the production of hydrogen peroxide at these potentials as indicated by the ring currents in Figure 12 and with the second peak in the voltammetry curves (Figure 2) which indicates a

second reduction process at ∿ -0.6V. This reduced form of the catalyst seems to be less effective for the 4 e^- reduction process.

Figure 15 shows a plot of N I_D/I_R vs. $1/f^{1/2}$ for the potential range where some peroxide is detected. The marked deviation from linear behavior at low values of $1/f^{1/2}$ may be caused by shaft eccentricity; i.e., wobble. Independent of whether the deviations at low values of $1/f^{1/2}$ are real or an experimental artifact, the data indicate a large potential dependent value of N I_D/I_R at infinite rotation rate. This suggests a parallel mechanism. Such behavior appears reasonable since a portion of the ordinary pyrolytic graphite surface is probably not blocked by the adsorbed Fe-TSP and will support the O_2 reduction principally to peroxide. The Fe-TSP may still support at least in part the overall 4 e^- reduction.

The effect of pH on the O_2 reduction currents on Fe-TSP adsorbed on ordinary pyrolytic graphite was studied and the results are summarized in Tafel plots in Figure 16. The solubility of O_2 in the different solutions varies slightly and is considerably smaller for the 1M NaOH solution according to the different I_L obtained for a given rotation rate. This will give different concentrations of O_2 for the different solutions used, which will be reflected directly in the currents since the process is first order in O_2. The plots in Figure 16, however, include a correction for these differences since the parameter $I/(I_L-I)$ is independent of the O_2 concentration in solution for first order kinetics. This is verified in Figure 17 where data obtained in O_2 and air saturated solutions also have been plotted in the form $I/(I_L-I)$ vs. E and superimpose.

The linear region of low polarization in Figure 16 is strongly dependent on pH in contrast to the linear region of high polarization. The slopes of the lines in the pH range 13.8 to 10.8 are essentially the same and have values in the range -30 to -35 mV/decade. At lower pH values, these

slopes increase reaching a value of -65 mV/decade at pH = 4.4. It was not possible to obtain reproducible data at pH values lower than 4.4 since the Fe-TSP complex decomposes when the potential of the electrode is scanned cathodically in acid media. This is accelerated by the presence of O_2 and produces a rapid decrease in activity with time.

Plots of log $[I/(I_L-I)]$ vs. the overpotential $\eta = E - E_{rev}$ (Figure 18) shows some features which are not clearly evident in Figure 16. Figure 18 shows that the O_2 reduction process becomes more irreversible with decreasing pH (i.e., the process takes place at higher overpotentials in acid media). This is also observed on other carbon surfaces.

Another interesting feature that is clearly noted in this figure is that a limiting current is reached at log $[I/I_L-I)] = \sim 0.1$. This limiting current is associated with the pre-wave observed in the polarization curves (see Figure 12). This current is independent of pH for the whole range studied, independent of potential and first order in O_2 concentrations. A chemical limiting process with essentially potentially independent kinetics appears to be involved.

D. Reaction Order in OH^- at Low Polarization on Adsorbed Fe-TSP

Since the reaction is first order in O_2 concentration and the activity of water for the solutions of different pH is essentially constant, the rate of the reaction expressed as a kinetic current is

$$I_k = k\,[O_2]\,[OH^-]^m \qquad (7)$$

with the back reaction negligible. From eq. 7 the reaction order for OH^- is

$$m = \left(\frac{\partial \log I_K}{\partial \log [OH^-]}\right)_E = \left(\frac{\partial \log (I/(I_L-I)}{\partial \log [OH^-]}\right)_E \qquad (8)$$

where I_K is given by

$$I_K = I_L \frac{I}{(I_L - I)} \qquad (9)$$

for a first order reaction in O_2.

The plots of $\log[I/(I_L-I)]$ vs. $\log[OH^-]$ for the low polarization-Tafel linear region in Figure 18 yield straight lines in the pH range from 13.8 to 10.8 (Figure 19). In some instances it was necessary to extrapolate the low polarization-Tafel linear region to lower and higher values of $I/(I_L-I)$ to obtain the data in Figure 19.

The slopes of the linear portion of the curves in this figure range from -0.87 to -1.1 indicating a reaction order of -1 for OH^-. For pH values lower than 10.8 the order in OH^-decreases numerically. This correlates with an increase of the slope at low pH values in the Tafel plot of Figure 16.

Plots of the potential vs. pH for a constant $I/(I_L-I)$ values in the low polarization-Tafel linear regions yield straight lines for high pH values (13.8 to 8) with a slope of -30 mV/pH unit. This slope is compatible with a Tafel slope of -30 mV/decade and m = -1.

E. O_2 Reduction on Fe-TSP Adsorbed on SAPG

Essentially the same behavior has been observed for the disk currents for O_2 reduction on Fe-TSP adsorbed on SAPG. On the basis of the observed B values, the O_2 reduction appears to proceed virtually entirely by the overall 4 e^- process without any peroxide generation at potentials anodic to -0.5V. The B values indicate that peroxide generation becomes quite substantial at more cathdic potentials. O_2 reduction to peroxide or OH^- ion is grossly inhibited on the basal plane in the absence of the adsorbed complexes. Consequently this provides evidence that much of the peroxide is generated on the adsorbed Fe-TSP at more cathodic potentials and not just on the exposed graphite surface.

Tafel plots of $\log[I_K/(I_L-I)]$ vs. E are given in Figure 20 for Fe-TSP adsorbed on the basal plane of both SAPG and OPG. The chemical limiting currents are about 8 times smaller for the SAPG than for the ordinary pyrolytic graphite and ∿ twofold smaller for the high polarization-Tafel linear region but almost the same for the low polarization Tafel linear region.

From the cyclic voltammetry curves for these two surfaces the surface concentration of Fe-TSP on the SAPG is about 4 to 5 times smaller than that observed on ordinary pyrolytic graphite, expressed in terms of superficial area.

IV. Discussion

A. O_2 Reduction on Fe-TSP

On the basis of the experimental results for O_2 reduction on Fe-TSP adsorbed on the basal planes of SAPG and OPG, the mechanisms for O_2 reduction at low and high polarization are not the same. Evidence for this are the different Tafel slopes and pH dependence. The reaction at low polarization is strongly dependent on pH and has an order of -1 in OH^- ions over the pH range 13.8 to 10.8. In contrast, the process at high polarization is practically pH independent over the entire range studied (13.8 to 4.4). Both processes are first order in O_2.

The current potential data can be deconvoluted into two component processes as shown in Figure 21. The experimental current density i corresponds to the sum of the values for each individual process; i.e., $i(total)=i_a + i_b$. The process corresponding to i_b has been assumed to follow Tafel linearity only at more cathodic potentials and to approach zero current at potentials negative to the reversible value for the overall 4 e^- reduction in order to fit the experimental data. Such behavior may

occur if process b corresponds to a hydrogen peroxide producing reaction with the bulk peroxide concentration finite but very low(e.g., 10^{-7}M). Small residual currents were observed on the ring after several cathodic potential sweeps, providing evidence for such peroxide. The curve corresponding to i_b then approaches the reversible potential for the O_2/HO_2^-, OH^- couple for whatever is the bulk concentration of HO_2^-.

Mechanism at Low Polarization at pH > 8 (Mechanism I)

The more anodic peak in the voltammetry curves for Fe-TSP in Figure 2 occurs at potentials in the low polarization region (Figure 16) where deviations from Tafel linearly become evident. This suggests an involvement of the $[Fe(III)OH\ TSP]_{ads}/[Fe(II)\ TSP]_{ads}$ couple in the reaction mechanism responsible for this portion of the polarization curves. The following mechanism explains the O_2 reduction kinetics at pH > 8 for the region below the apparent chemical limiting current, corresponding to component i_a in Figure 21.

$$Fe^{III}OH_{ads} + e^- \rightleftharpoons Fe^{II}_{ads} + OH^- \qquad \text{fast} \qquad \text{(i)}$$

$$Fe^{II}_{ads} + O_2 \underset{k_{-2}}{\overset{k_2}{\rightleftharpoons}} (Fe^{III}\text{-}O_2^-)_{ads} \qquad \text{fast} \qquad \text{(j)}$$

$$(Fe^{III}\text{-}O_2^-)_{ads} + e^- \xrightarrow[rds]{k_3} \text{intermediates} \qquad \text{slow} \qquad \text{(k)}$$

where the TSP groups have not been shown for simplicity. Reaction k would then be followed by further fast steps yielding finally OH^- as the product of the O_2 reduction with a total of $4e^-$ per O_2 consumed. For this reaction scheme, the rate of the reaction expressed as a current density is given by:

$$i_a = 4Fk_3[Fe^{III}\text{-}O_2^-]\exp[-\tfrac{\alpha F}{RT}(E-E_o)] \qquad (10)$$

where $[Fe^{III}-O_2^-]$ is the surface concentration of this adsorbed species, α is the symmetry factor, and k_3 is the rate constant at the standard electrode potential for reaction k; i.e., at $E = E_o$.

Applying the Nernst equation to reaction i and assuming ideal behavior

$$E + E_o - \frac{RT}{F} \ln \frac{[Fe^{II}]\ (OH^-)}{[Fe^{III}OH]} \tag{11}$$

where [ ] represent surface concentration and ( ) solution phase concentration. Brown and Anson (20) have called attention to the deviation of adsorbed complexes from Nernst behavior when using concentrations rather than activities or coverage dependent standard free energies or E_o values (i.e., non-Langmuir behavior). The deviations, however, should be small in the present work since the concentration of the adsorbed macrocyclic, and hence, the change in charge density are low.

The surface concentration of the Fe species can be expressed in terms of coverage θ; i.e.,

$$[Fe^{II}] = \theta m;\ 0 < \theta < 1 \tag{12}$$

$$[Fe^{III}OH] = (1-\theta)m \tag{13}$$

where m is the total surface concentration of Fe-TSP species. Introducing eqs. 12, 13 into eq. 11 and solving for θ,

$$\theta = \frac{(OH^-)^{-1} \exp - \frac{F}{RT}(E-E_o)}{1 + (OH^-)^{-1} \exp - \frac{F}{RT}(E-E_o)} \tag{14}$$

Assuming steady state for step j, the concentration of $[Fe^{III}-O_2^-]$ adsorbed species is given by:

$$[Fe^{III}-O_2^-] = \frac{\vec{k}_2[O_2]\theta m - i_a}{\vec{k}_2} \tag{15}$$

Replacing $[Fe^{III}O_2^-]$ in eq. 10 with eq. 15, replacing k_3/k_{-2} by K and rearranging,

$$i_a = 4Fk_2(O_2)\theta m \quad \frac{K \exp - \frac{\alpha F}{RT}(E-E_o)}{1 + K \exp - \frac{\alpha F}{RT}(E-E_o)} \tag{16}$$

When $\theta \to 1$ and $K \exp \frac{-\alpha F}{RT} (E-E_o) \gg 1$, then i approaches a limiting value, given by

$$(i_a)_L = 4Fk_2(O_2)m \tag{17}$$

The coverage θ of Fe^{II}-TSP approaches one at potentials cathodic to E_o; i.e., all Fe-TSP on the surface becomes Fe^{II}-TSP. For example, when $E-E_o$ = -0.1V, θ = 0.93; and when $E-E_o$ - -0.2 V, θ = 0.999.

Combining eqs. 10-16 and rearranging:

$$i_a = (i_a)_L \quad \frac{(OH^-)^{-1} K \exp - [(1+\alpha) \frac{F}{RT} (E-E_o)]}{[1 + (OH^-)^{-1} \exp - \frac{F}{RT} (E-E_o)] [1 + K \exp - \frac{\alpha F}{RT}(E-E_o)]} \tag{17a}$$

This equation predicts the essential features of the experimental data below the high polarization-Tafel linear region in the pH range from 8.7 to 13.8. The reaction rate is first order in (O_2), -1 in (OH^-) and predicts a limiting current density $(i_a)_L$ that is directly proportional to O_2 concentration, to Fe-TSP surface concentration and independent of pH. The quantity $(i_a)_L$ is not a diffusing limiting current density but is due to a potential insensitive chemical process, reaction j, which becomes rate controlling when the Fe^{II} species approach saturation and the cathodic polarization has increased the rate of reaction k to a relatively high value. According to this proposed mechanism, the Tafel slope for the linear Tafel region of i_a should be $-RT/[1+\alpha)F)$. The value of the slope will depend on the value of α. For α = 0.5 the slope is -RT/(1.5F) or -40 mV/ decade and

for $\alpha = 1$ is $-RT/(2F)$, or -30 mV/decade as compared with an experimental value of $\sim$ -35 mV/decade. A Tafel linear region of slope $-RT/[(1+\alpha)F]$ should be observed only if both terms $(OH^-)^{-1} \exp -\frac{F}{RT}(E-E_o)$ and $K \exp -\frac{\alpha F}{RT}(E-E_o)$ are small compared to unity. If either term becomes much larger than unity while the other is still very small compared to unity, a second Tafel linear region of higher slope should be observed. For $(OH^-)^{-1} \exp -\frac{F}{RT}(E-E_o) \gg 1$ and $K \exp -\frac{\alpha F}{RT}(E-E_o) \ll 1$, then the Tafel slope of $-RT/(\alpha F)$ or $\sim$-120 mV/decade would be expected while for the reverse situation, the slope should be -60 mV/decade. Neither of these slopes has been observed at high pH. The limiting current $(i_a)_L$ is achieved with a gradual change in the slope and an intermediate linear region is not observed. It is possible that the log linear region occurs only close to the limiting current $(i_a)_L$ over too small a potential range to be evident.

Acid-base Equilibrium of Fe-TSP

At more acid pH it is necessary to consider the acid-base equilibrium:

$$Fe^{III}OH^- \underset{}{\overset{K_B}{\rightleftharpoons}} Fe^{III} + OH^- \qquad (l)$$

The redox process may be represented as

$$\begin{array}{ccc} Fe^{III}OH & \overset{e^-}{\rightleftharpoons} & Fe^{II} + OH^- \\ \uparrow\downarrow K_B & \nearrow & \\ Fe^{III} + OH^- & & \end{array} \qquad (m)$$

or alternatively

$$\begin{array}{ccc} Fe^{III}\text{-}OH^- + H^+ & \overset{+e^-}{\rightleftharpoons} & Fe^{II} + H_2O \\ \uparrow\downarrow K_A & \nearrow & \\ Fe^{III} + H_2O & & \end{array} \qquad (n)$$

with

$$K_B = \frac{[Fe^{III}]\,(OH^-)}{[Fe^{III}OH]} = \frac{1-x}{x}(OH^-) \qquad (18)$$

with x the fraction of the surface adsorbed Fe^{III} complete as $Fe^{III}OH$.

Solving for x,

$$x = \frac{(OH^-)/K_B}{1 + (OH^-)/K_B} \tag{19}$$

Expressing the concentrations as coverage, the Nernst equation for reaction m becomes

$$E = E_o - \frac{RT}{F} \ln \frac{\theta(OH^-)}{(1-\theta)x} \tag{20}$$

Solving eq. 20 for θ,

$$\theta = \frac{x(OH^-)^{-1} \exp - \frac{F}{RT}(E-E_o)}{1 + x(OH^-)^{-1} \exp - \frac{F}{RT}(E-E_o)} \tag{21}$$

Mechanism at Low Polarization in Acid Media (Mechanism II)

It is possible that the uptake of O_2 by Fe^{II} becomes rate controlling when the pH of the solution is lowered. The following mechanism for acid media is proposed:

$$[Fe^{II}] + O_2 \xrightarrow{k_2} [Fe^{III}O_2^-] \qquad \text{slow} \qquad (n)$$

$$[Fe^{III}O_2^-] + H^+ + e^- \rightarrow \text{intermediate} \qquad \text{fast} \qquad (o)$$

where Fe^{II} is generated by reaction m. The rate of the reaction expressed as a current is

$$i_a = 4Fk_2[Fe^{II}](O_2) \tag{22}$$

Expressing $[Fe^{II}]$ as coverage, using θ from eq. 21, and replacing $4Fk_2m(O_2)$ by $(i_a)_L$ as before, the final expression becomes (21)

$$i_a = (i_a)_L \frac{x(OH^-)^{-1} \exp - \frac{F}{RT}(E-E_o)}{1 + x(OH^-)^{-1} \exp - \frac{F}{RT}(E-E_o)} \tag{23}$$

This mechanism predicts a Tafel slope of -F/RT or -60 mV/decade at 25°C. It also predicts a limiting current directly proportional to (O_2) and to the surface concentration of [Fe-TSP] species. This limiting current is independent of pH.

The terms x and $(OH^-)^{-1}$ are interdependent according to eq.19. At alkaline pH values, $[OH^-] >> K_B$ and x in eq. 19 becomes unity. At more acid pH values, the behavior of eq. 19 will depend on the value of K_B. Figure 3 predicts an approximate value for the acid dissociation constant of $K_A \approx 10^{-4}$ and hence $K_B \approx 10^{10}$.

When $(OH^-) = \sim 10^{-10}$M, x - 0.5 and when $(OH^-) << K_B$, x = 0. According to this, at pH < 4 eq. 20 becomes independent of (OH^-), and

$$x(OH^-)^{-1} = \frac{1/K_B}{1 + (OH^-)/K_B} = 1/K_B \qquad (24)$$

Equation 23 becomes

$$i_a = (i_a)_L \frac{K_B^{-1} \exp - \frac{F}{RT}(E-E_o)}{1 + K_B^{-1} \exp - \frac{F}{RT}(E-E_o)} \qquad (25)$$

Equations 19 and 23 fit the experimental observation (Figure 19) that at low pH, i_a has relatively little or no pH dependence.

Mechanism I and II are expected to be competitive in the pH range between 10 and 4. This would explain the gradual change in the Tafel slope over this pH range. Equations 19 and 23 do not include a correction for the mass transport of O_2 to the electrode surface. This correction is small in the current range where i_a is predominant. At high current densities the correction can be made with the equation

$$(O_2) = \frac{(i_L - i)}{i_L}(O_2)_{bulk} \qquad (26)$$

where i_L corresponds to the diffusion limiting current density. At

more cathodic potentials the fraction of the current corresponding to peroxide generation becomes quite substantial. Since this fraction is potential dependent, i_L also becomes potential dependent. The value at any particular potential can be evaluated from the B values calculated from the $1/I$ vs. $1/f^{1/2}$ plots (Figure 14).

Mechanism at High Cathodic Polarization (Mechanism III)

Tafel slopes close to -120 mV/decade observed at high polarizations strongly suggest that a first one-electron transfer step becomes rate controlling at those potentials with mechanistic features analogous to those for Co-TSP. The process becomes practically pH independent as shown in the Tafel plots of Figure 16. The rate of reaction can then be expressed by:

$$i_b = 4Fkm\theta(O_2) \exp - \frac{\alpha F}{RT}(E-E_o) \qquad (27)$$

or

$$i_b = 4Fkm\theta(O_2)_{bulk} \frac{i_L - i}{i_L} \exp - \frac{\alpha F}{RT}(E-E_o) \qquad (27a)$$

where eq. 27a contains the correction for mass transport of O_2 from the data.

The pH independence of the process indicates that protons or OH^- ions are not involved before or in the rate determining step.

A mechanism which explains the behavior at high polarization is as follows:

$$(M^{II}\text{-TSP})_{ads} \xrightarrow[e]{O_2} [(M^{III}\text{-TSP})\text{-}O_2^-]_{ads} \qquad \text{fast} \qquad (p)$$

$$[(M^{III}\text{-TSP})\text{-}O_2^-]_{ads} \xrightarrow{e^-} [(M^{II}\text{-TSP})\text{-}O_2^-]_{ads} \qquad \text{slow} \qquad (q)$$

$$[(M^{II}\text{-TSP})\text{-}O_2^-]_{ads} \xrightarrow[HOH]{e^-} (M^{II}\text{-TSP})_{ads} + O_2H^- \qquad \text{fast} \qquad (r)$$

Reactions p and q may be either separate steps as shown or a single step. This same mechanism probably is also operative for O_2 reduction on $(Co\text{-}TSP)_{ads}$ and is to be preferred to the mechanism suggested earlier (9) since it accounts for the zero reaction order dependence on OH^- ion concentration.

A redox mechanism similar to mechanisms I and II is not observed on the adsorbed Co-TSP. This is probably related to the differences in the redox properties of Fe-TSP and Co-TSP. At pH 1, the Co^{II}/Co^{III}-TSP couple occurs at +0.78 V vs. SCE and the Fe^{II}/Fe^{III} couple at +0.40 V. Therefore it should be much easier for O_2 in binding to the transition metal of the TSP complex to oxidize Fe^{II} to Fe^{III} than Co^{II} to Co^{III}.

Some caution must be exercised in comparing the behavior of the adsorbed M-TSP at monolayer levels with that of thick layers of the corresponding phthalocyanine on carbon substrates or that of the bulk complex. Nonetheless the experimental results of the present study may explain the different Tafel slope found by various authors for O_2 reduction on metal chelates. For example the Tafel slopes reported for O_2 reduction on iron complexes at $\sim$ 25°C include -30 (6-8), -45 (30) and -60 (31) mV/decade. For cobalt chelates, slopes of -40 (37), -60 (4) and -120 (9,10,30,33) mV/decade have been found. On the basis of the present work, this distribution of Tafel slopes appears to result from differences in the redox potentials and pK's of the couples and pH of the electrolytes. Despite the obvious importance of the redox properties of the surface species, relatively few authors have placed much emphasis on them in their studies (see e.g., 2-4, 34).

Manassen and Bar-Ilan (2) measured the redox potentials of metal phthalocyanines by solubilizing them in tetrabutyl ammonium perchlorate solutions. Randin (3) used the data for the homogeneous couple to rationalize the catalytic behavior of transition metal phthalocyanines

in alkaline solutions. Aside from the question of the redox potentials for the heterogeneous vs. homogeneous Fe phthalocyanine couple, the difference in pH is expected to shift the potential very substantially. Similar behavior has been observed for iron porphyrins (35) and vitamin B-12 (36).

Appleby and Savy (6-8) have reported Tafel slopes of -30 mV/decade for O_2 reduction on layers of Fe phthalocyanine on carbon in alkaline media with an OH^- reaction order of -1. This is similar to the results found in the present work with Fe-TSP on graphite. It is very likely that the potential of the Fe^{II}/Fe^{III} phthalocyanine couple falls in the same range of potential where these slopes are observed. A recently reported value for the Fe^{II}/Fe^{III} phthalocyanine couple by Beck (4) at pH = 0 is +0.7V vs. SHE. If we assume that the pK_A of $Fe^{III}Pc\text{-}OH$ is approximately 4, then at pH = 14 the redox potential for iron phthalocyanine should be approximately +0.10V, which is in the region of the -30 mV/decade slope.

In summary the present study provides an explanation for the different experimental results reported in the literature in terms of:

1. One mechanism is predominant for alkaline media with a Tafel slope close to F/2RT. These two mechanisms can become competitive at intermediate pH values. This explains the gradual increase of the slopes at more acid pH values found by several authors (6-8,37) and in the present work. These two mechanisms are controlled by the M^{II}/M^{III} couples and are only observed when the potential of these redox couples is close to that where O_2 reduction takes place. This is the case for Fe-TSP and on the basis of literature data also for Fe-Pc and Co-TAA (6,8,37).
2. At potentials far cathodic to those of the transition metal redox couple, a redox type of mechanism is not operative since all of the catalyst

is in the lower valency state and the chemical step $M^{II} + O_2 \rightarrow M^{III}O_2^-$ does not occur because the formation of the M^{III} species is thermodynamically unfavorable even in the O_2 adduction. In this case a first one-electron transfer step becomes rate controlling via a different pathway and the Tafel slopes are close to $RT/(\alpha F)$ (-120 mV/decade for $\alpha = 0.5$). This is the case for adsorbed Fe-TSP and Co-TSP in the present study and for Co-TAA, Co-Pc, Ni-Pc and Cu-Pc reported in the literature (30,33,37).

Acknowledgement

The authors acknowledge the support of segments of this research by the U. S. Office of Naval Research, the Department of Energy, and the Electric Power Research Institute. One author expresses appreciation to the Organization of American States which provided a graduate fellowship to one of the authors (JZ) during 1976-77.

References:

1. H. Jahnke, M. Schonborn and G. Zimmermann in "Organic Dyestuffs as Catalysts for Fuel-Cells," Topics in Current Chemistry, 61, 135 (1976).

2. J. Masassen and Bar-Ilan, J. Catalysis, 17, 86 (1970).

3. J. P. Randin, Electrochim. Acta, 19, 83 (1974).

4. F. Beck, J. Appl. Electrochem., 7, 239 (1977).

5. A. J. Appleby and M. Savy, Natl. Bur. Stand. Spec. Publ., 455, 241 (1976).

6. A. J. Appleby, J. Fleisch and M. Savy, J. Catal., 44, 281 (1976).

7. A. J. Appleby and M. Savy, Electrochim. Acta, 22, 1315 (1977).

8. A. J. Appleby and M. Savy, in Proc. Symp. Electrode Materials and Processes for Energy Conversion and Storage, J. D. E. McIntyre, S. Srinivasan and F. W. Will, eds., pp. 247-264, 1977.

9. J. Zagal, R. Sen and E. Yeager, J. Electroanal. Chem., 83, 207 (1977) and references therein.

10. R. Sen, J. Zagal and E. Yeager, Inorg. Chem., 16, 3379 (1977).

11. J. Zagal, P. Bindra and E. Yeager, "Oxygen Reduction on Metal Phthalocyanines Adsorbed on Graphite Electrodes", Paper 539, National Meeting, The Electrochemical Society, Seattle, May 21-26, 1978.

12. W. J. Albery and S. Bruckenstein, Trans. Faraday Soc., 62, 1920 (1966).

13. F. Beck, Ber. Bunsenges., 77, 353 (1973).

14. J. Manassen, J. Catal., 33, 133 (1974).

15. H. Sigel, P. Waldmeir and B. Prijs, Inorg. Nucl. Chem. Letters, 7, 161 (1971).

16. K. Fenkart and C. H. Brubaker, J. Inorg. Nucl. Chem., 3245 (1968).

17. A. B. P. Lever and J. P. Wilshire, Inorg. Chem., 17, 1145 (1978).

18. A. Damjanovic, M. R. Tarasevich and V. Y. Filinovskii, Electrokhimiya, 5, 1218 (1969).

19. H. S. Wroblowa, Y. C. Pan and G. Razumney, J. Electroanal. Chem., 71, 195 (1976).

20. A. P. Brown and F. C. Anson, Anal. Chem., 49, 1589 (1977).

21. J. Zagal, Ph.D. Thesis, Case Western Reserve University, 1978.

22. J. P. Randin and E. Yeager, J. Electroanal. Chem., 36, 257 (1972).

23. I. Morcos and E. Yeager, Electrochim. Acta, 15, 953 (1970).

24. W. G. Wilke, "Solubilities of Inorganic and Metal Organic Compounds", Vol. II, 4th Ed., Amer. Chem. Soc., Washington, D.C., p. 1219 (1969).

25. K. Gubbins and R. Walker, J. Electrochem. Soc., 112, 469 (1965).

26. R. Davies, G. Horvath and C. W. Tobias, Electrochim. Acta, 12, 287 (1967).

27. Handbook of Chemistry and Physics, 54th Ed., C. R. C. Press (1973).

28. V. G. Levich, "Physiochemical Hydrodynamics", English Translation, Prentice Hall, Englecliffs, N.J., (1962).

29. J. C. Huang, R. K. Sen, and E. Yeager, J. Electrochem. Soc., 126, 786 (1979).

30. M. Savy, P. Andro, C. Bernard and G. Magner, Electrochim. Acta, 18, 191 (1973).

31. M. Savy, C. Bernard and G. Magner, Electrochim. Acta, 20, 383 (1975).

32. J. Newman, J. Phys. Chem., 70, 1327 (1966).

33. E. Yeager, P. Bindra, N. Doddapaneni, J.C. Huang, R.K. Sen, and J. Zagal, Final Report, EPRI E.M.-505, Case Western Reserve University, Cleveland, Ohio, June (1977).

34. J. Ulstrup, J. Electroanal. Chem., 79, 171 (1977).

35. A.P. Brown, C. Koval and F.C. Anson, J. Electroanal. Chem., 72, 379 (1976).

36. D. Lexa and J.M. Saveant, J. Am. Chem. Soc., 98, 2652 (1976).

37. H. Behret, H. Binder, W. Clauberg and G. Sandstede in "On the Mechanism of the Electrocatalytic Oxygen Reduction with Particular Regard to Metal Chelates", in Proc. Symp. on Electrode Materials and Processes for Energy Conversion and Storage, J.D.E. McIntyre, S. Srinivasan and F.G. Will, Eds., pp. 519-536, 1977.

38. J. Weber and D.H. Busch, Inorg. Chem., 4, 469 (1965).

39. J.P. Randin and E. Yeager, J. Electrochem. Society 118, 711 (1971).

40. H. Meier, U. Tschirwitz, E. Zimmerhacki, W. Albrecht, and G. Zeittler, J. Phys. Chem., 81, 712 (1977).

41. D. Behar, G. Czapski, J. Rabani, L.M. Dorfman, and H.A. Schwarz, J. Phys. Chem., 74, 3209 (1970).

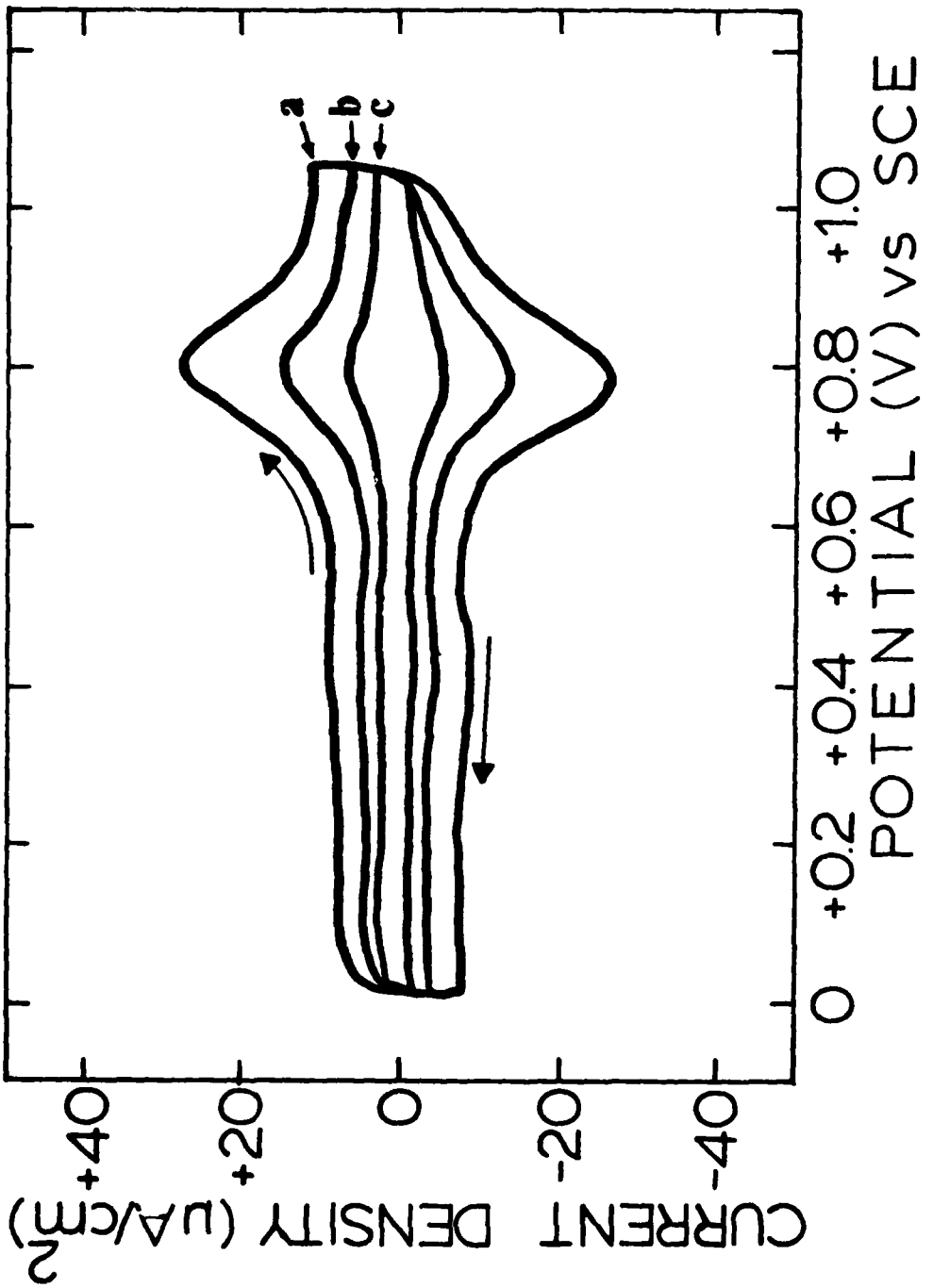

Figure 1. Cyclic voltammograms at different scanrates for Co-TSP adsorbed on SAPG, Electrolyte: 0.05 M H_2SO_4. (No Co-TSP in solution; obtained with hood to block electrolyte at edge of disk).

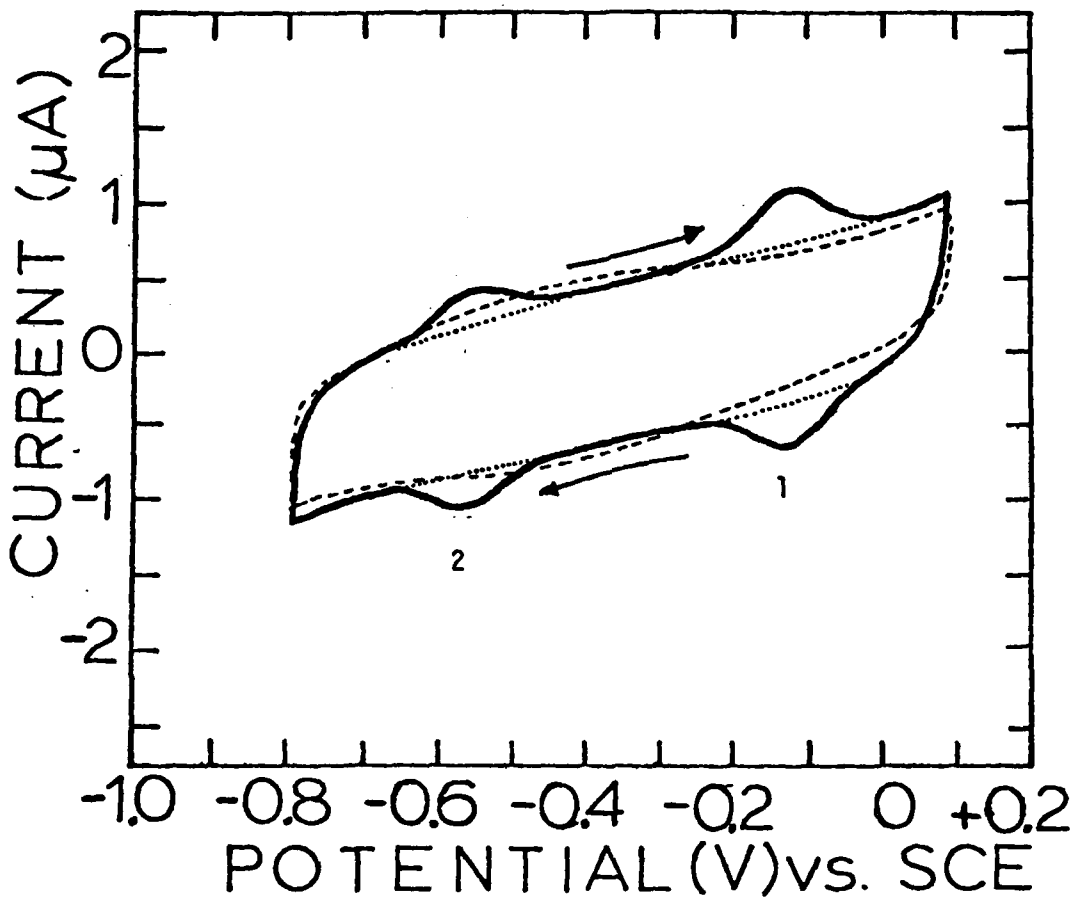

Figure 2. Cyclic voltammograms with (solid line) and without (dashed line) Fe-TSP pre-adsorbed on SAPG. Supporting electrolyte: 0.1M NaOH, He saturated. Scan rate: 500m V/s. (Obtained without hood).

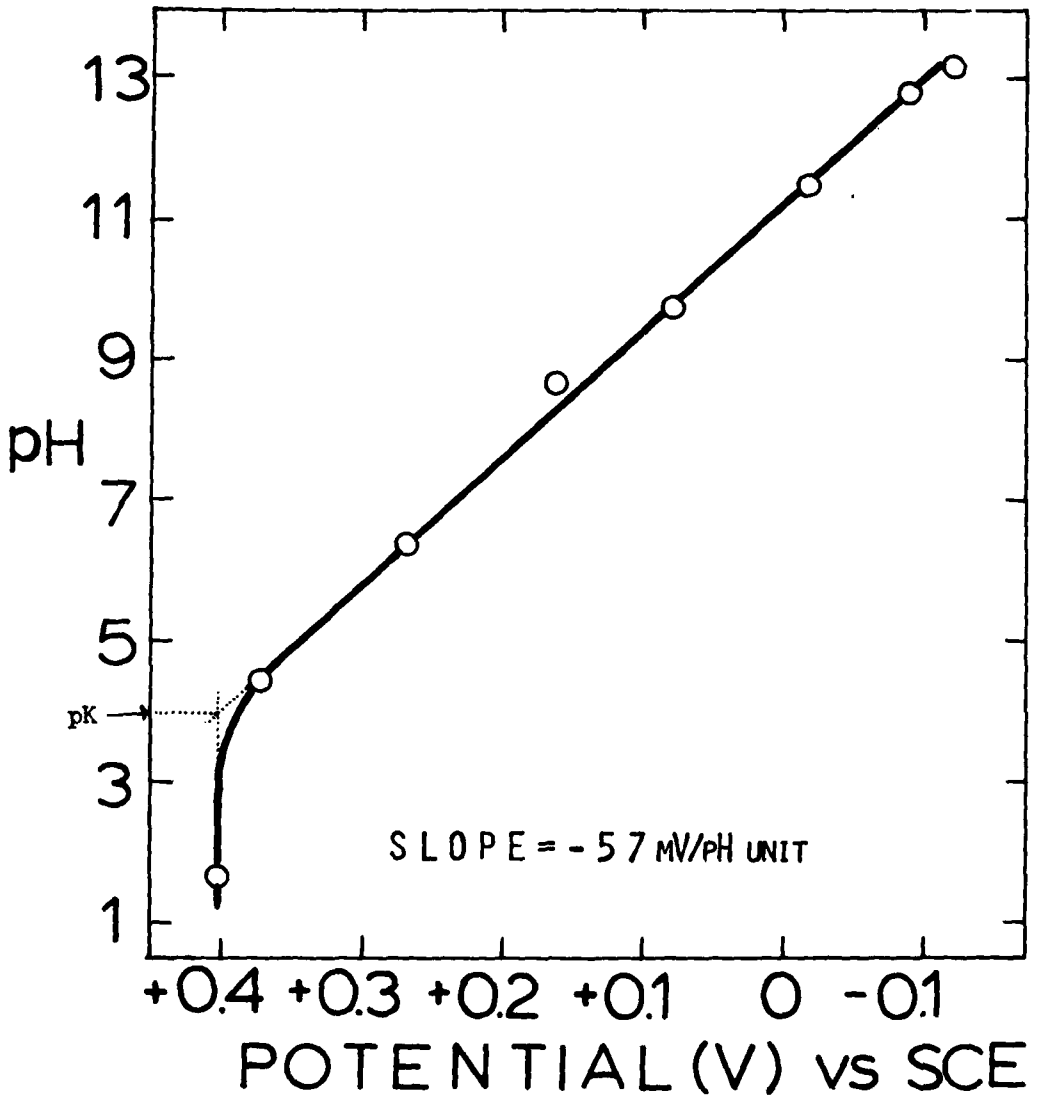

Figure 3. pH dependence of the potential of peak 1 in the voltammetry (see Fig. 2) for Fe-TSP adsorbed on OPG.

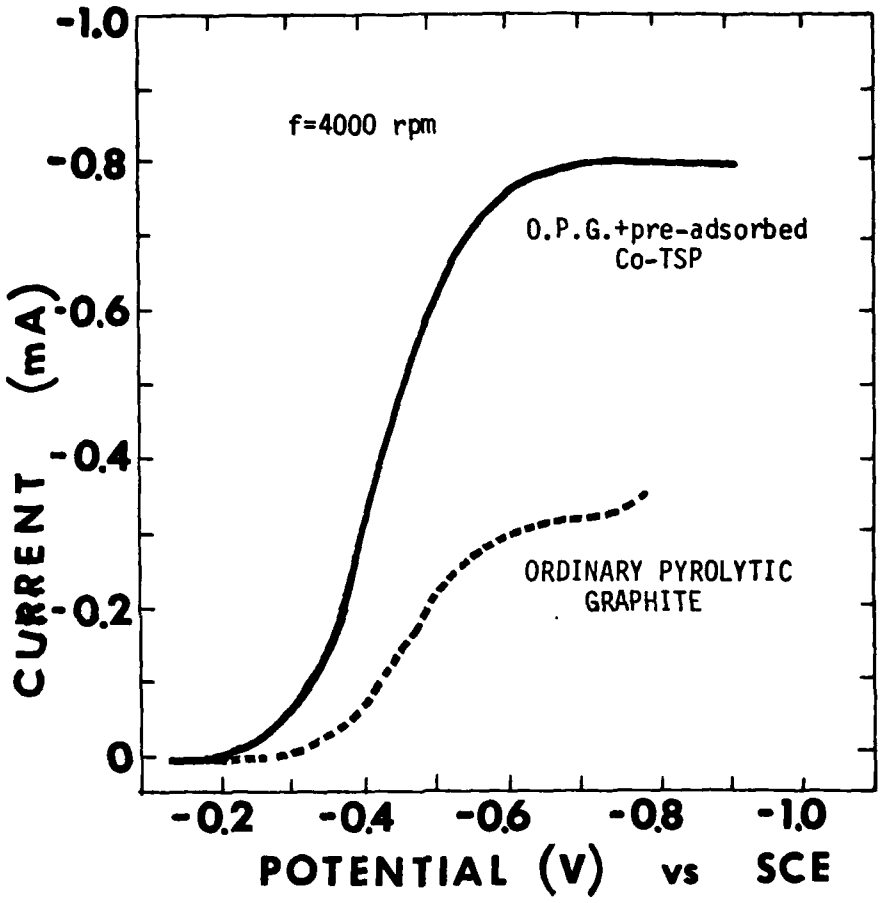

Figure 4. O_2 reduction in 0.1M NaOH on the rotating disk electrode with (solid line) and without (dashed line) Co-TSP pre-adsorbed on OPG. Rotation rate: 4000 rpm; scan rate: 10m V/s.

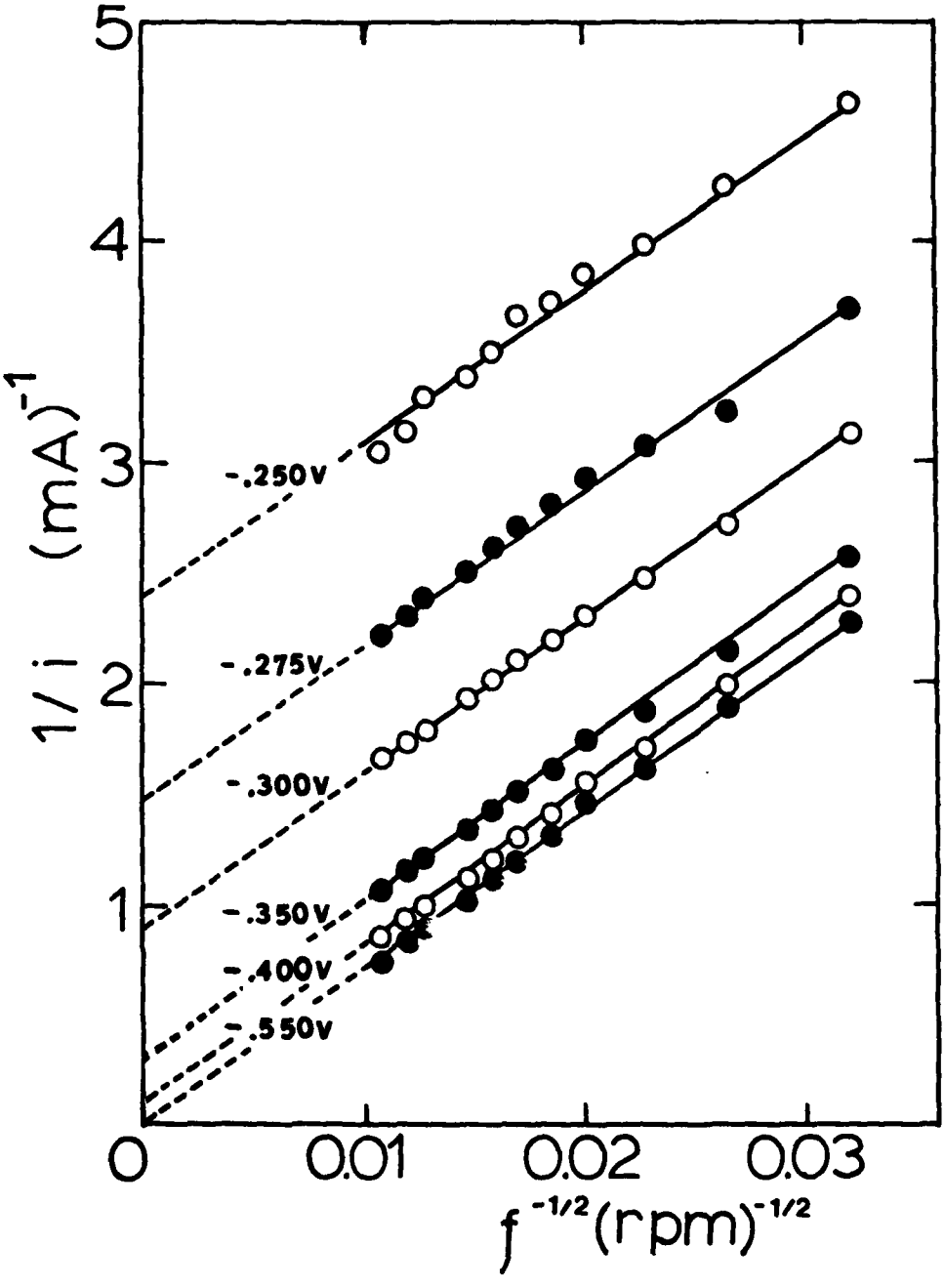

Figure 5. Plots of $1/I$ vs $1/f^{1/2}$ for Co-TSP adsorbed on SAPG in 0.1M NaOH + 10^{-6}M Co-TSP.

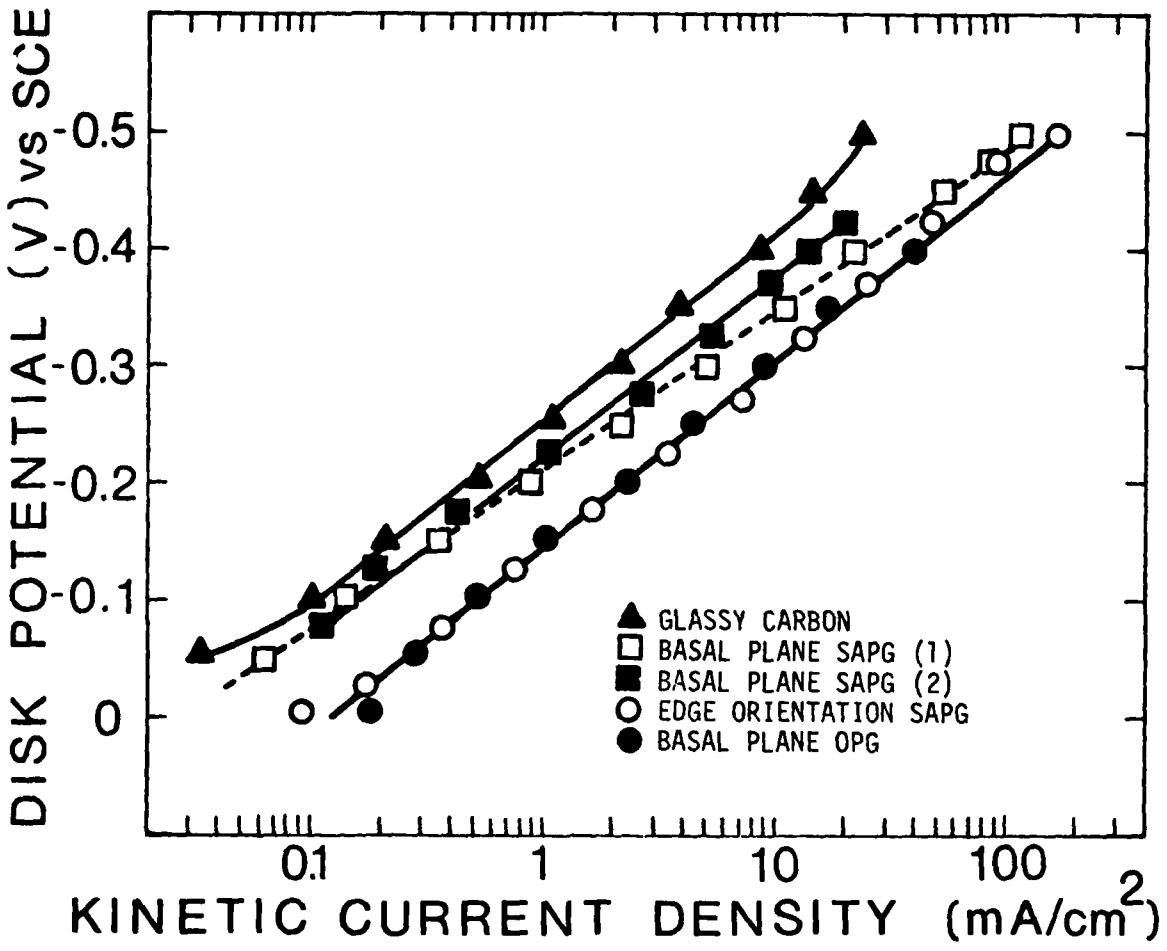

Figure 6. Tafel plots for O_2 reduction on Co-TSP adsorbed on various carbon surfaces. Kinetic current densities corrected for diffusion. Electrolyte: 0.05M H_2SO_4 + 10^{-5}M Co-TSP; f=2600 rpm.

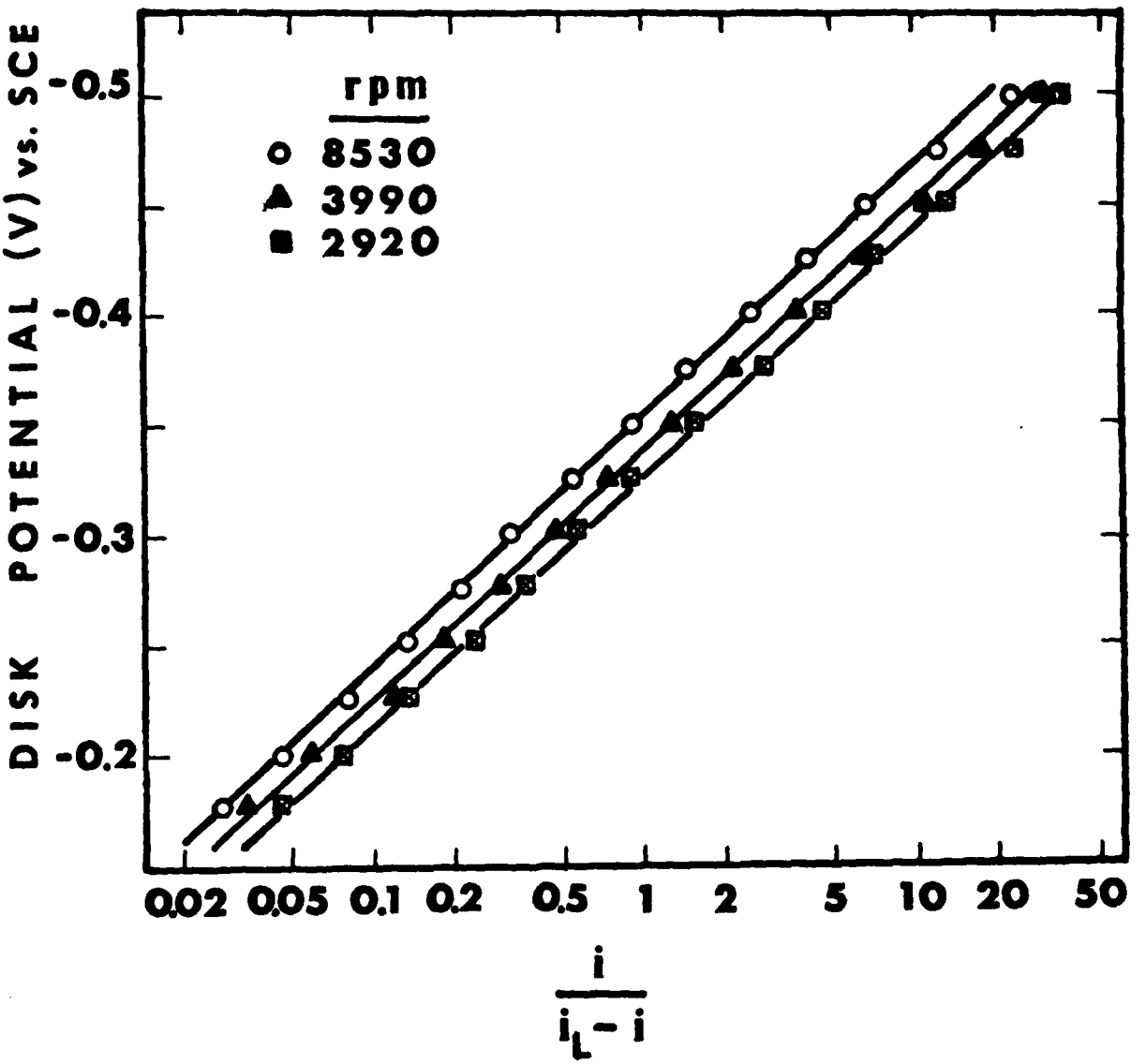

Figure 7. Tafel plot of log $[i/(i_L-i)]$ vs. E for O_2 reduction at various rotation rates for Co-TSP adsorbed on SAPG in 0.1M NaOH.

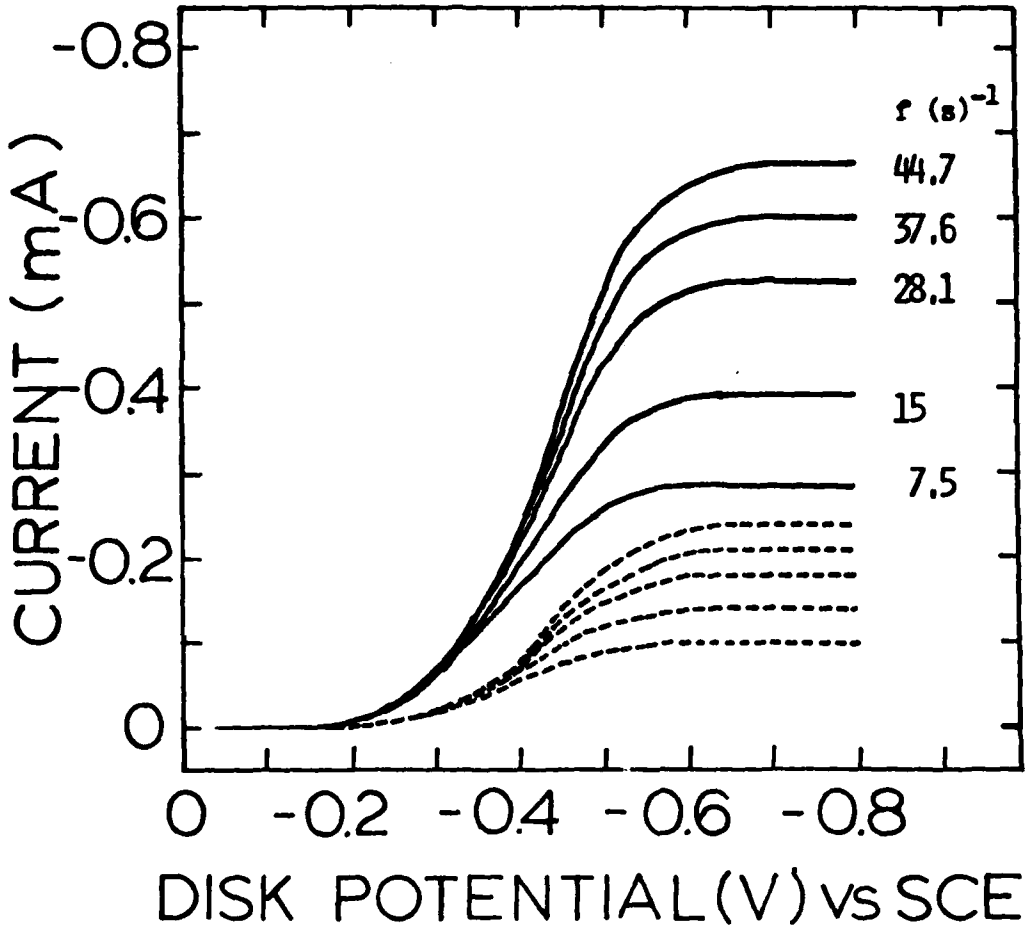

Figure 8. Rotating ring-disk data for O_2 reduction on Co-TSP pre-adsorbed on OPG in 0.1M NaOH. Disk current indicated by solid lines; ring current by dashed lines. Scan rate: 10m V/s. Ring potential: + 0,1V vs SCE. Ring current are anodic. Collection efficiency: $N = 0.38$.

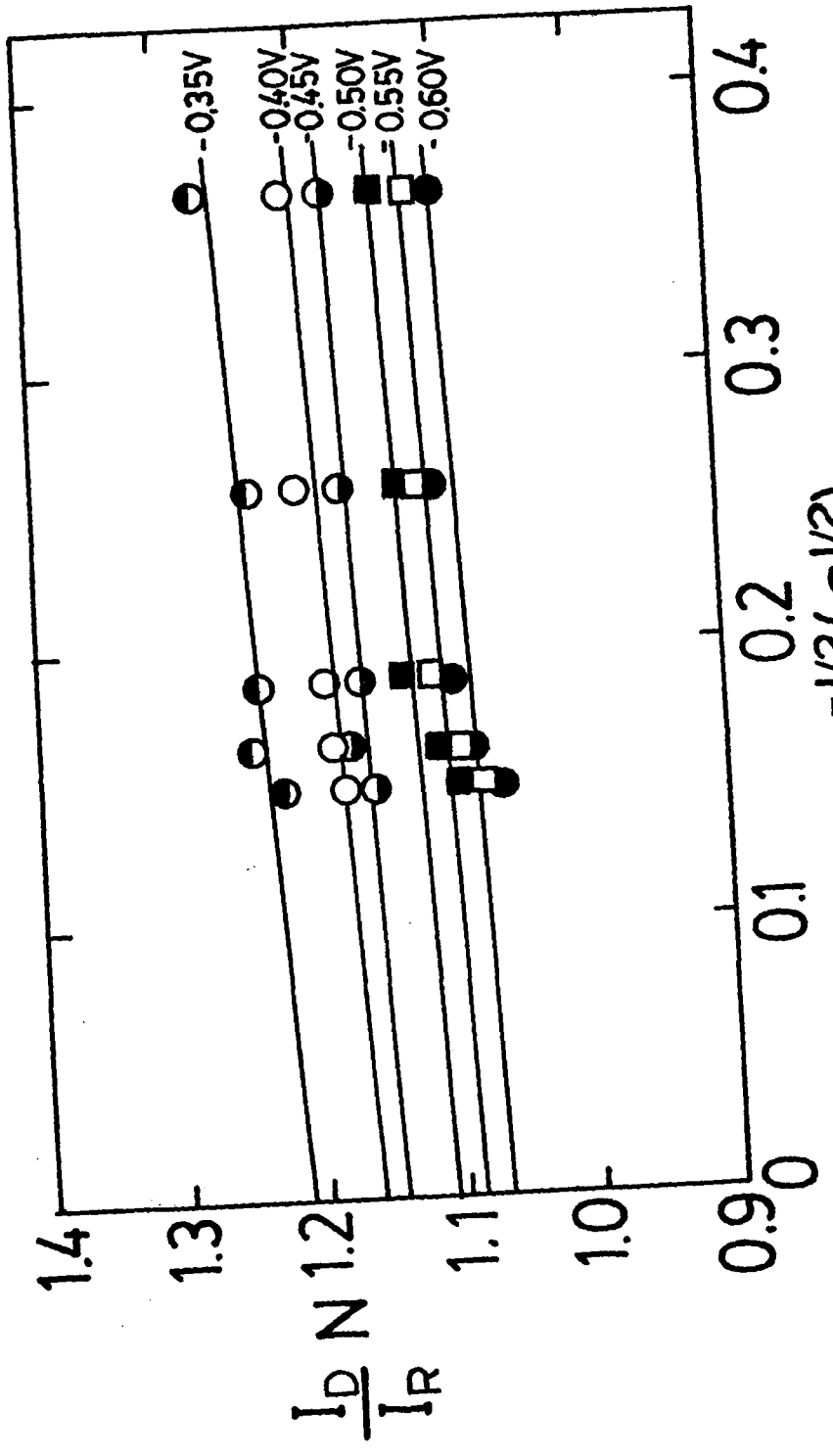

Figure 9. Plots of I_D N/I_R vs. $1/f^{1/2}$, constructed from ring-disk data in Fig. 8.

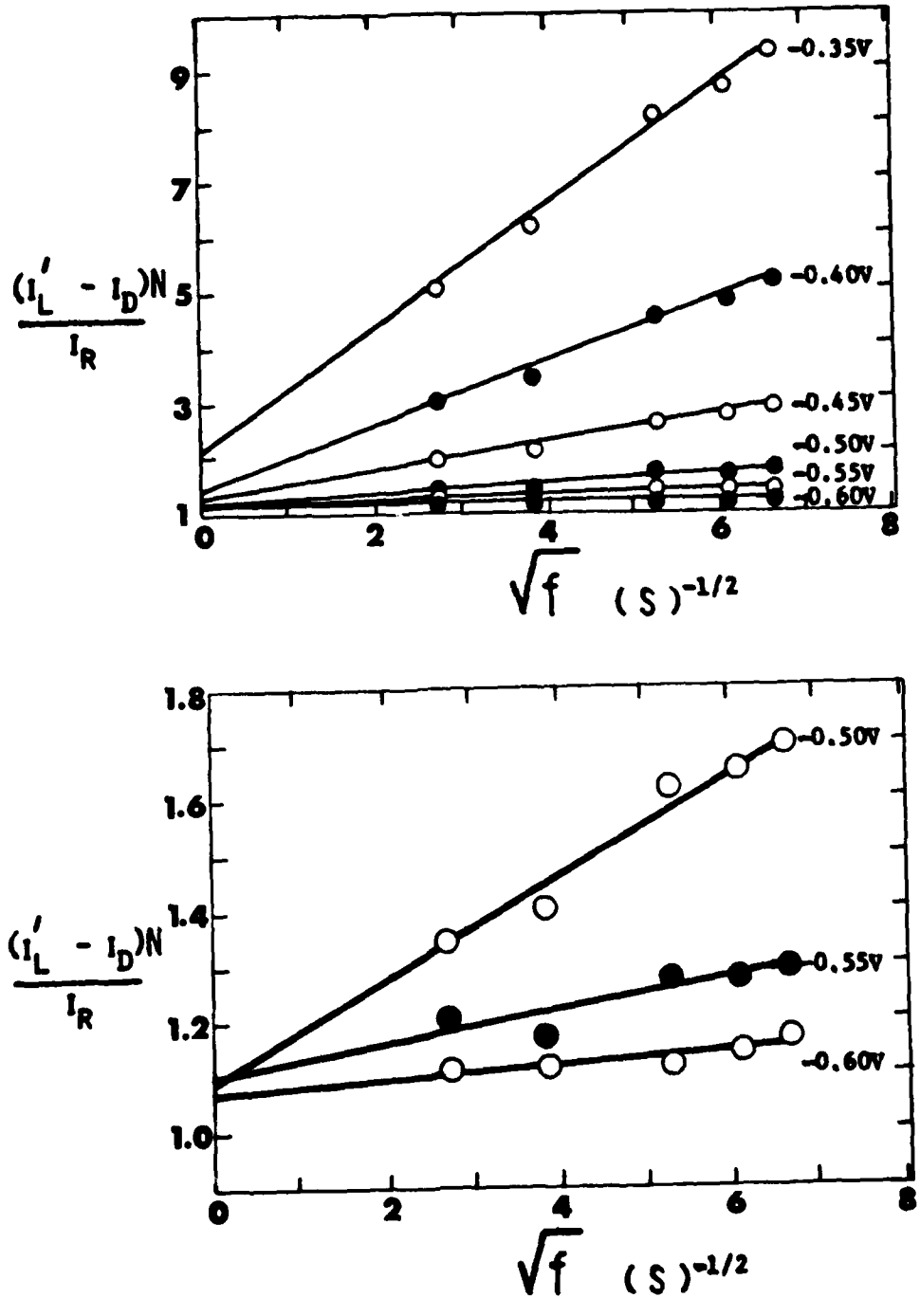

Figure 10. Plots of $(I'_L - I_D)\ N/I_R$ vs $1/f^{1/2}$ constructed from ring-disk data in Fig. 8.

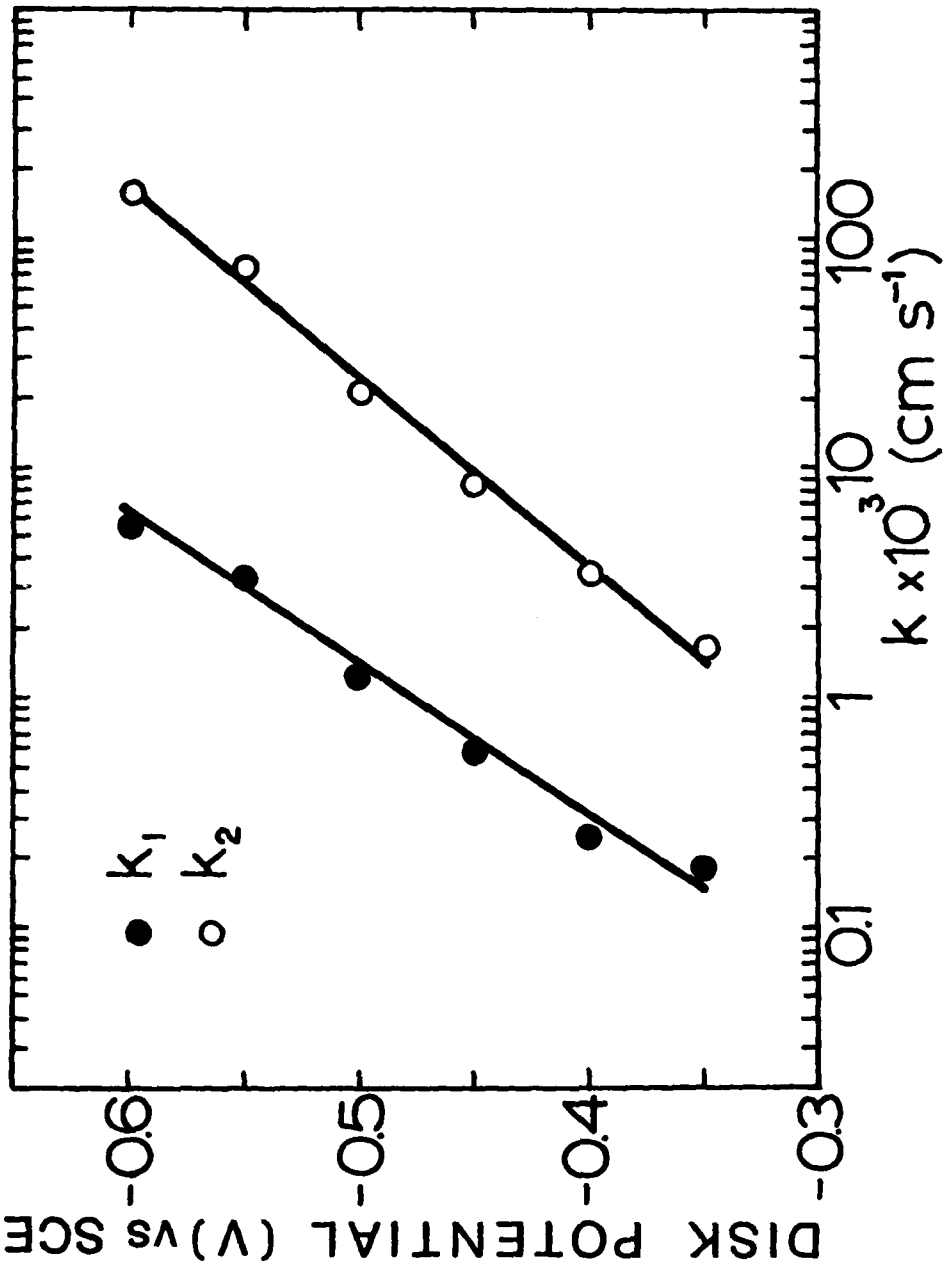

Figure 11. Potential dependence of the heterogeneous rate constants for the $4e^-$ reduction (k_1) and $2e^-$ reduction (k_2) of O_2 on Co-TSP adsorbed on OPG in 0.1 M NaOH.

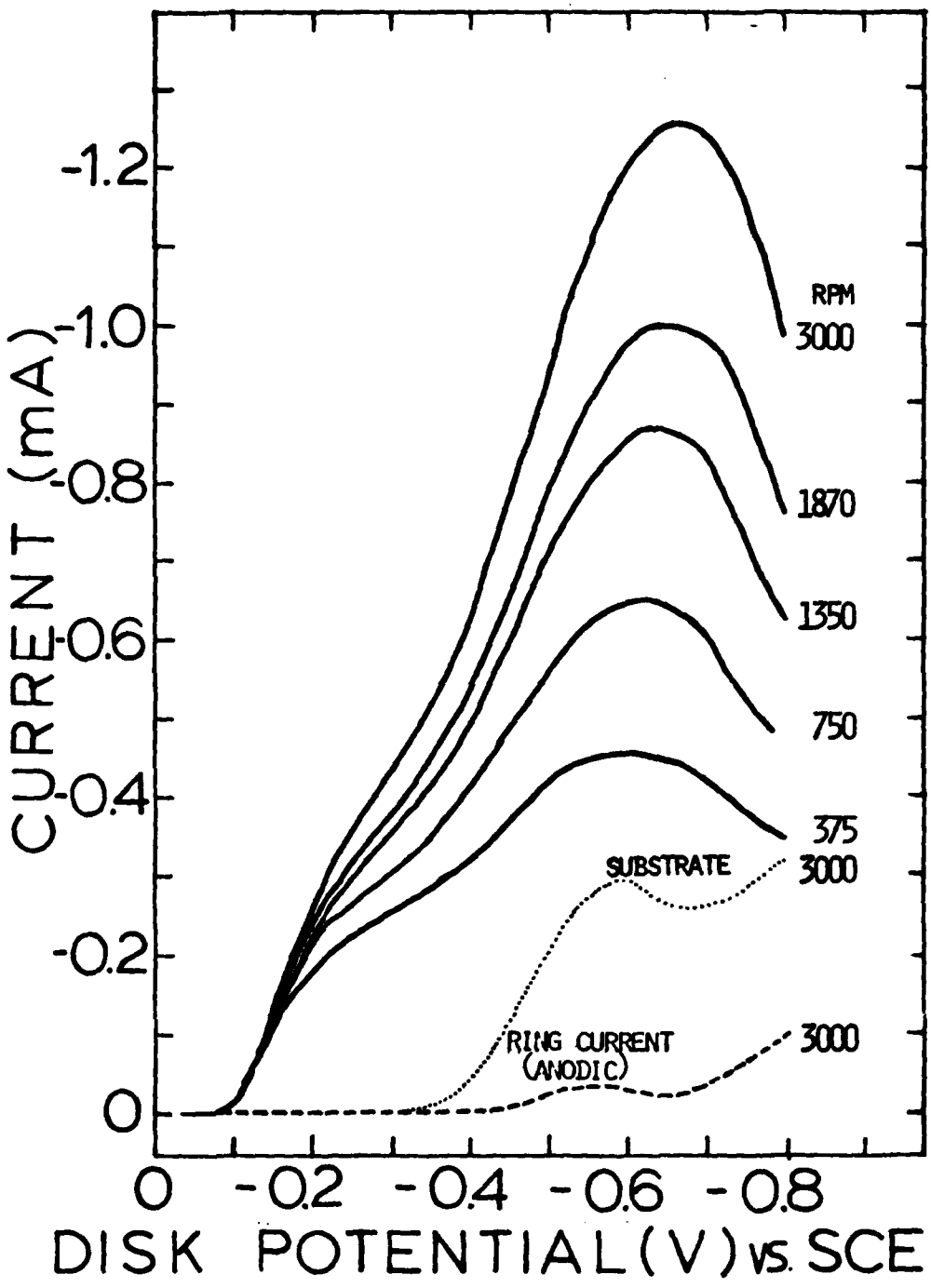

Figure 12. Rotating ring-disk data for O_2 reduction on Fe-TSP pre-adsorbed on the disk of OPG. Disk currents in solid lines; ring currents in dashed lines; current on OPG disk without Fe-TSP, dotted line. Electrolyte: 0.1 M NaOH. Scan rate: 5m V/s. Ring potential: +0.1V vs SCE. Collection efficiency: N = 0.38.

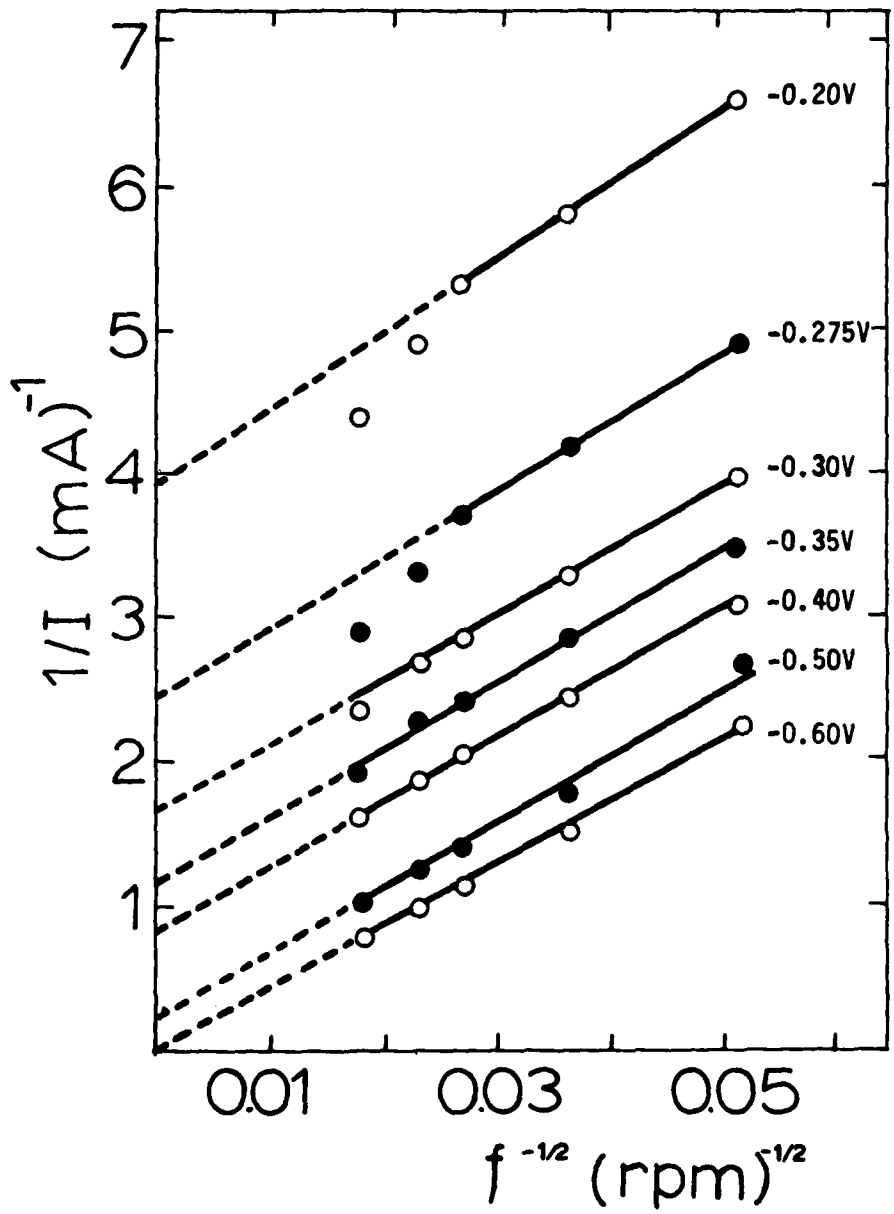

Figure 13. 1/I vs $1/f^{1/2}$ plot for currents in the potential region more anodic than -600 mV vs SCE for conditions in Fig 12.

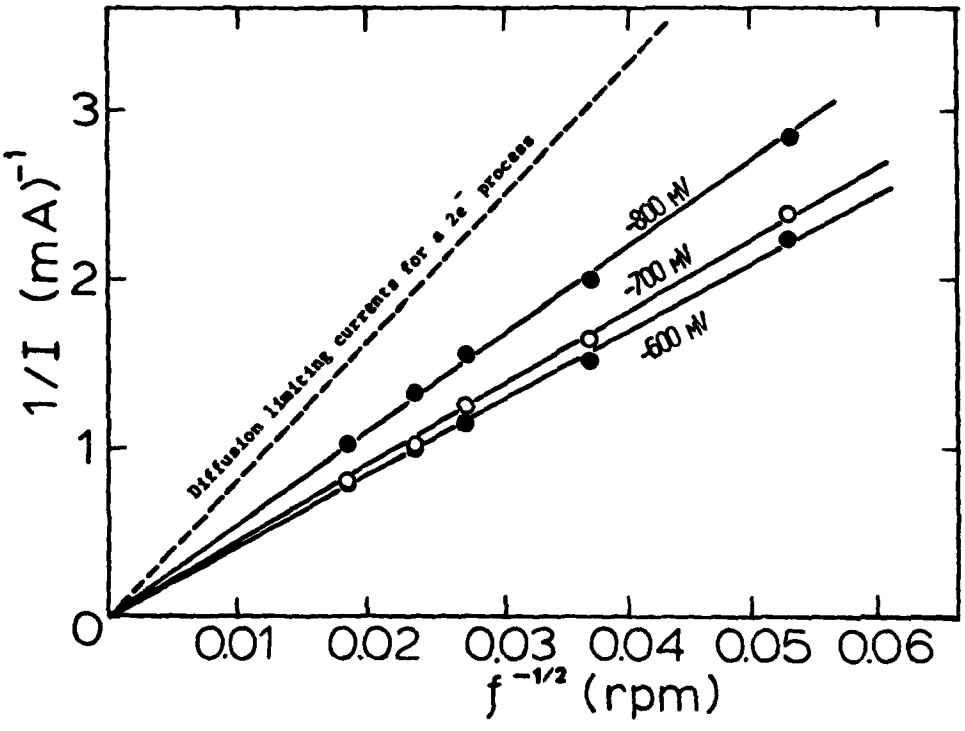

Figure 14. 1/I vs $1/f^{1/2}$ plot for currents in the potential region more cathodic than -600m V vs SCE for condition in Fig. 12.

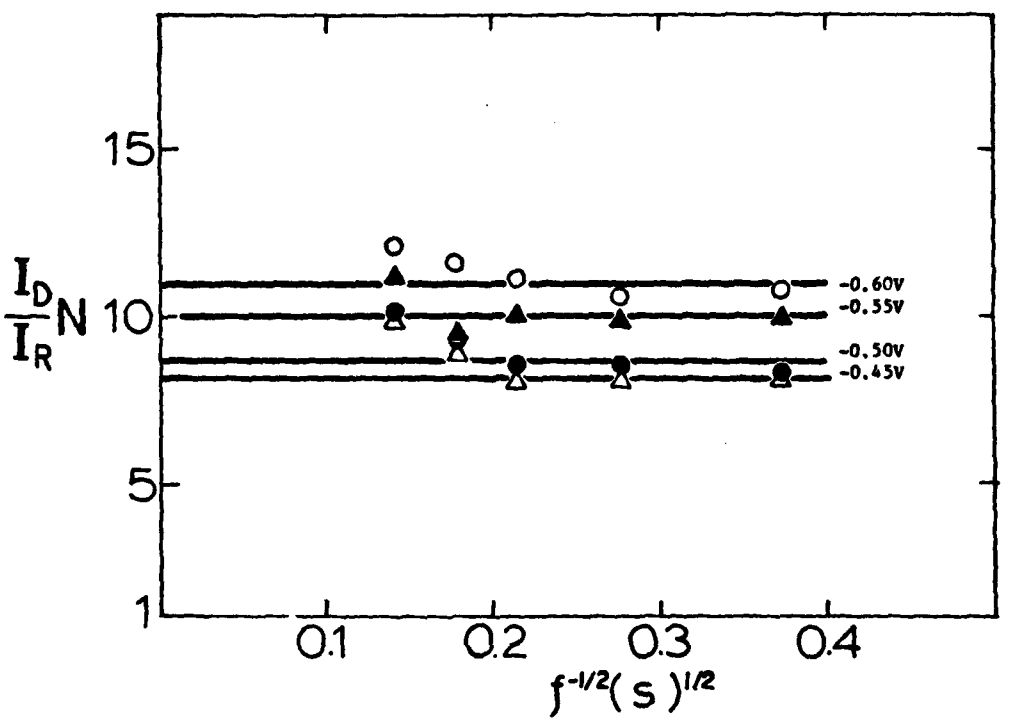

Figure 15. Plot of N I_D/I_R vs $1/f^{1/2}$ for various disk potentials for conditions indicated in Fig. 12.

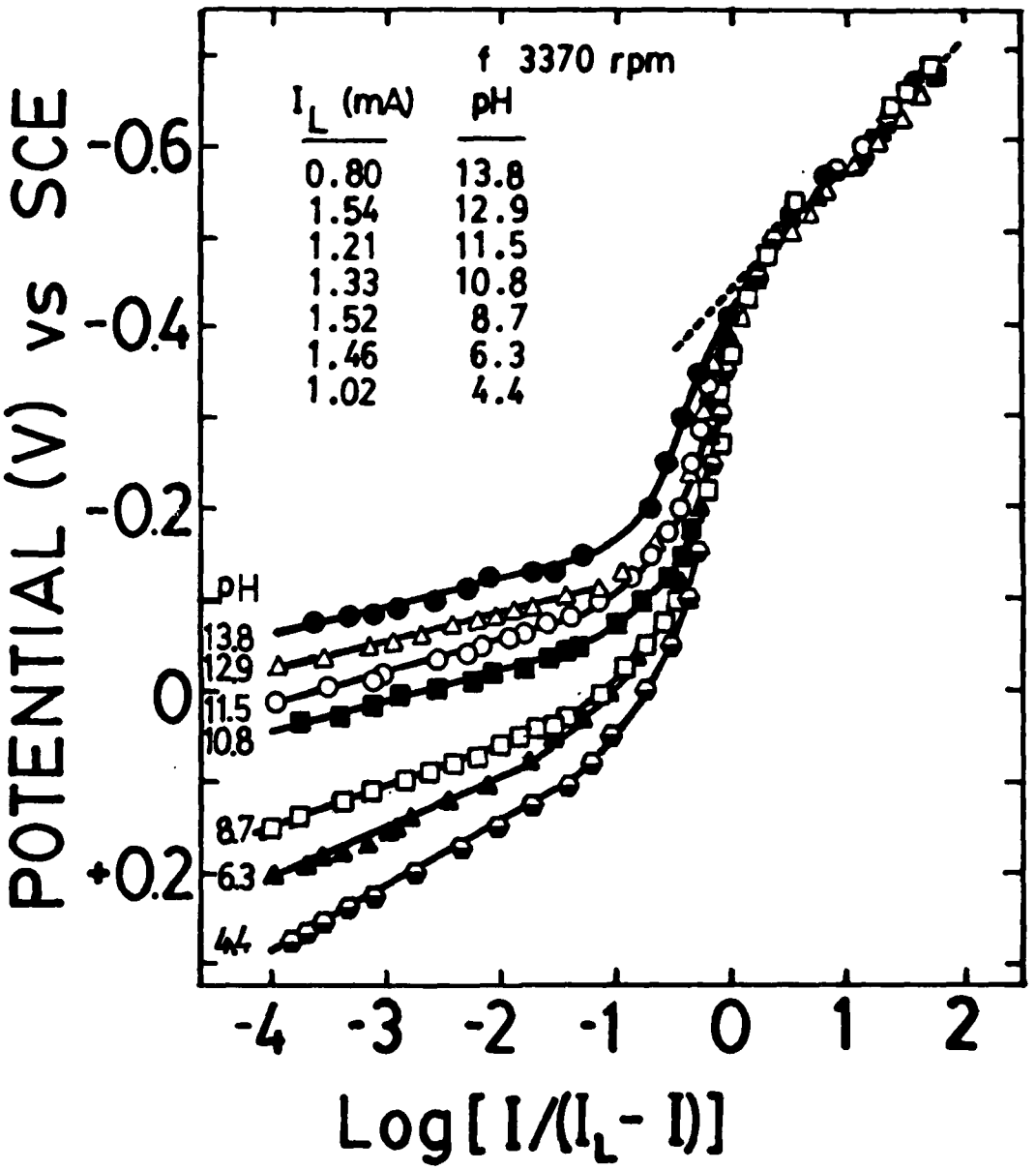

Figure 16. Tafel plots for O_2 reduction on Fe-TSP adsorbed on OPG in solution of various pH values. Rotation rate: 3370 rpm

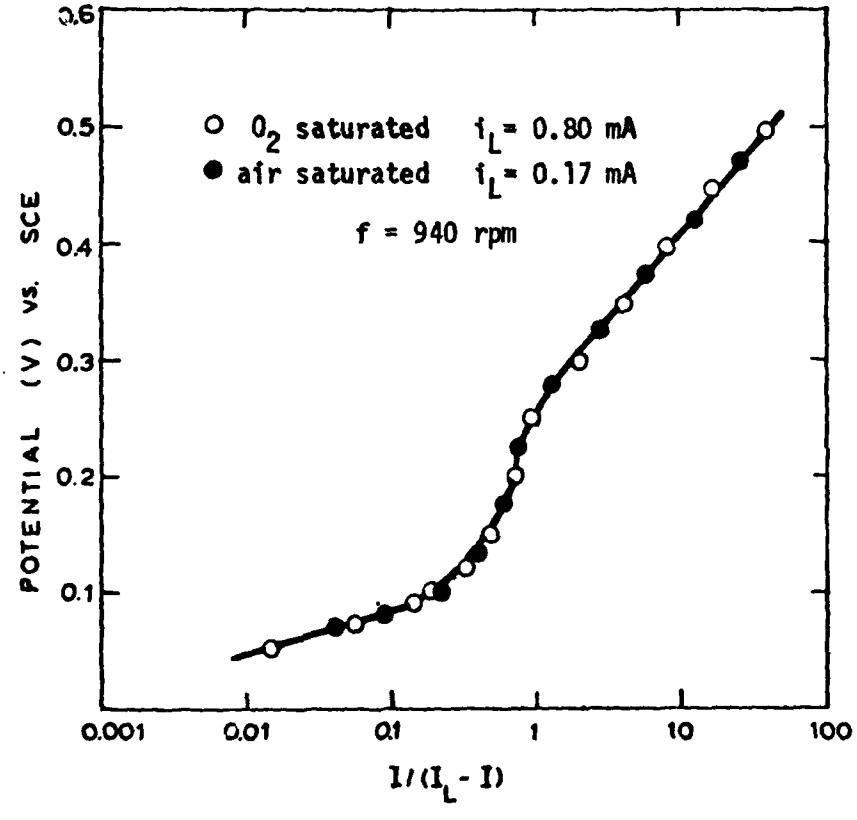

Figure 17. Tafel plots of log $[I/(I_L-I)]$ vs E for 0_2 reduction on Fe-TSP on OPG using 0_2 saturated and air-saturated 0.1M NaOH.

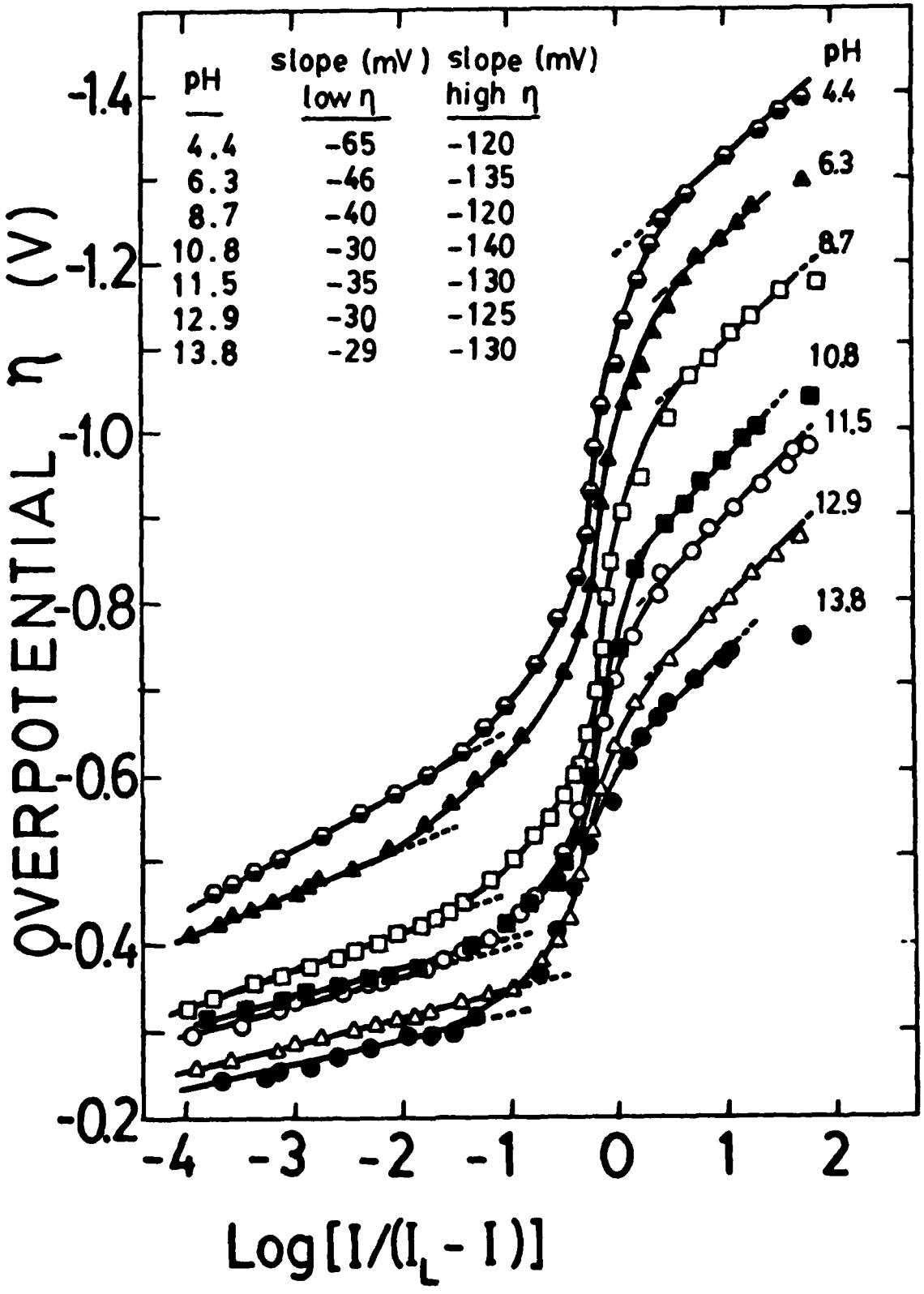

Figure 18. Tafel plots of overpotential vs log $[I/I_L-I)]$. Conditions are the same as for Fig. 16.

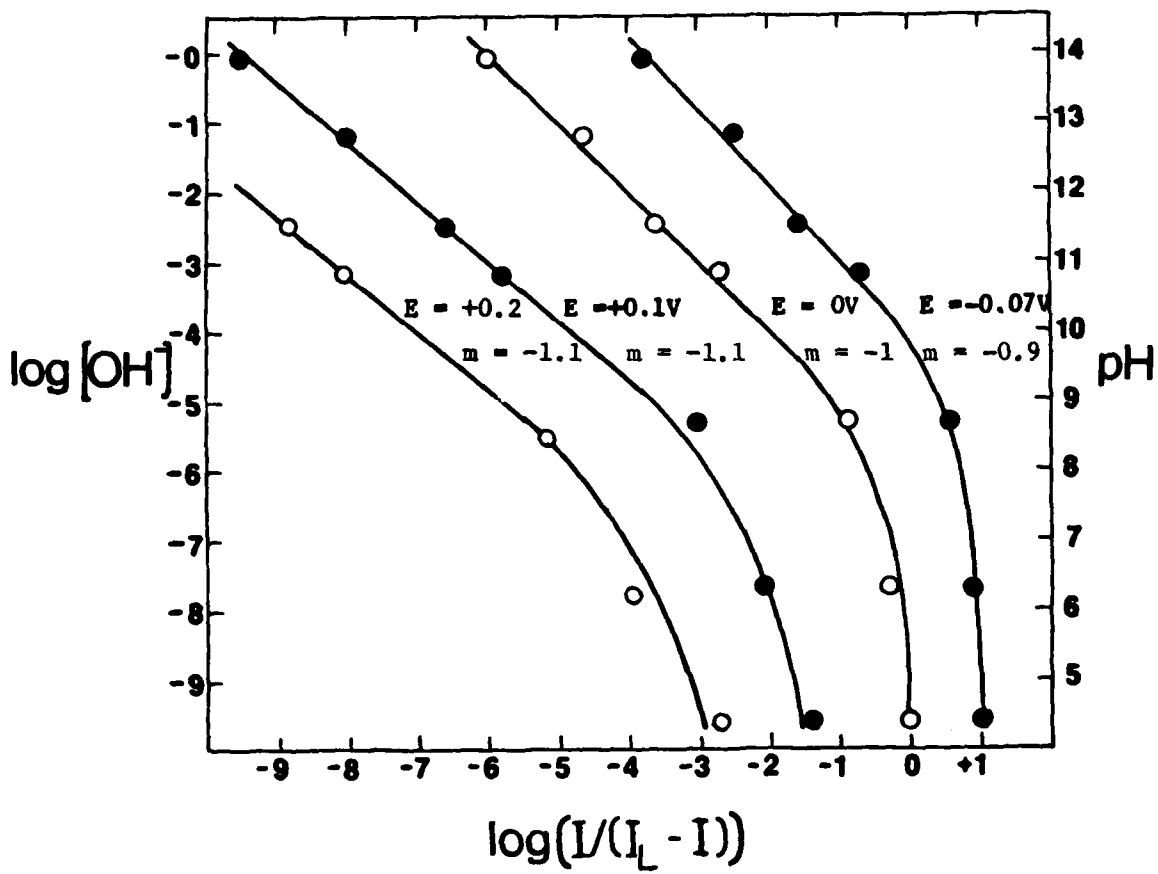

Figure 19. Plots of log $[I/(I_L-I)]$ vs log $[OH^-]$ for values of $I/(I_L-I)$ taken from the Tafel linear region of low polarization in Fig 16, extrapolated, if necessary, at a constant potential.

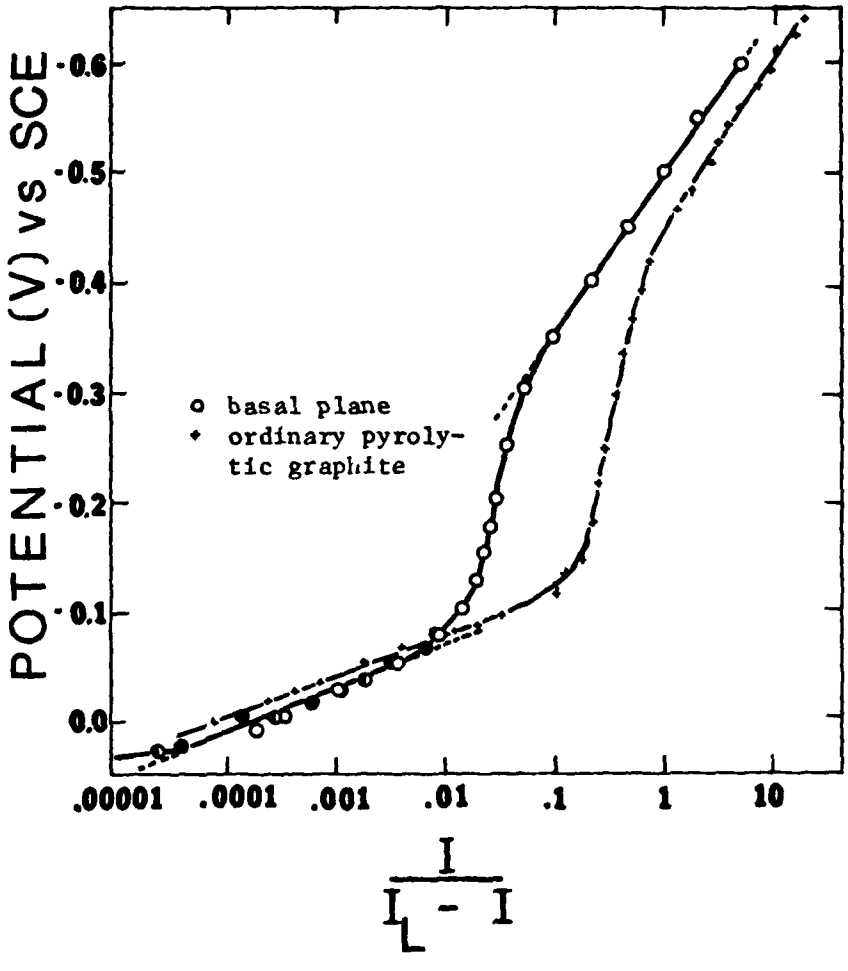

Figure 20. Tafel plot of log $[I/(I_L-I)]$ vs E for O_2 reduction in Fe-TSP adsorbed on SAPG and OPG at f=3000 rpm in 0.1 M NaOH.

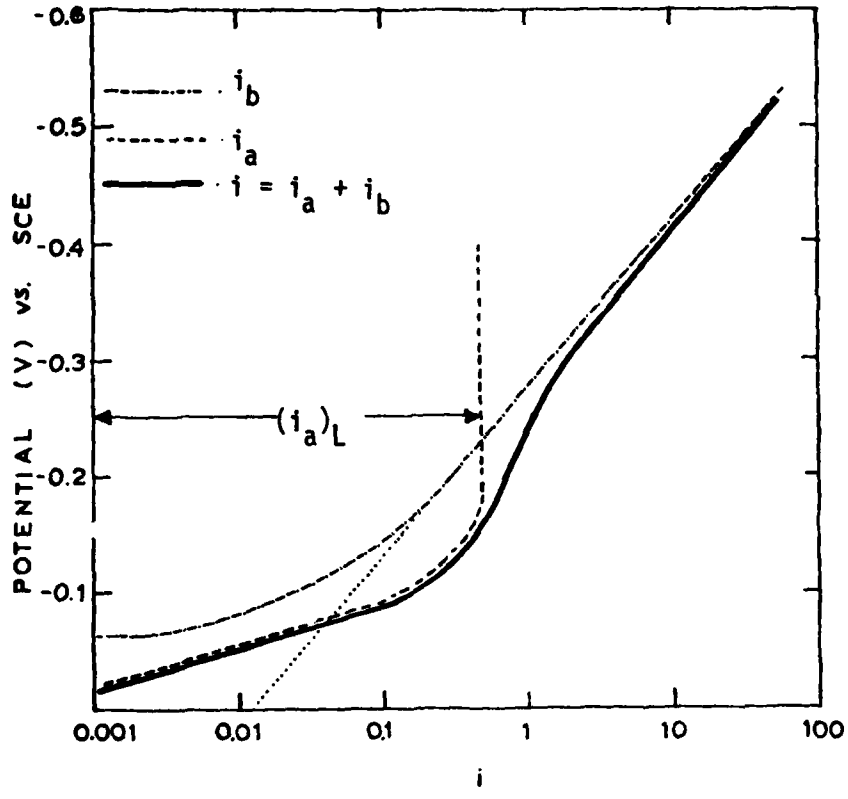

Figure 21. Graphical representation of the combination of two processes for O_2 reduction on adsorbed Fe-TSP in basic media.

TECHNICAL REPORT DISTRIBUTION LIST, GEN

	No. Copies
Office of Naval Research Attn: Code 472 800 North Quincy Street Arlington, Virginia 22217	2
ONR Branch Office Attn: Dr. George Sandoz 536 S. Clark Street Chicago, Illinois 60605	1
ONR Branch Office Attn: Scientific Dept. 715 Broadway New York, New York 10003	1
ONR Branch Office 1030 East Green Street Pasadena, California 91106	1
ONR Branch Office Attn: Dr. L. H. Peebles Building 114, Section D 666 Summer Street Boston, Massachusetts 02210	1
Director, Naval Research Laboratory Attn: Code 6100 Washington, D.C. 20390	1
The Assistant Secretary of the Navy (R,E&S) Department of the Navy Room 4E736, Pentagon Washington, D.C. 20350	1
Commander, Naval Air Systems Command Attn: Code 310C (H. Rosenwasser) Department of the Navy Washington, D.C. 20360	1
Defense Documentation Center Building 5, Cameron Station Alexandria, Virginia 22314	12
Dr. Fred Saalfeld Chemistry Division Naval Research Laboratory Washington, D.C. 20375	1
U.S. Army Research Office Attn: CRD-AA-IP P.O. Box 1211 Research Triangle Park, N.C. 27709	1
Naval Ocean Systems Center Attn: Mr. Joe McCartney San Diego, California 92152	1
Naval Weapons Center Attn: Dr. A. B. Amster, Chemistry Division China Lake, California 93555	1
Naval Civil Engineering Laboratory Attn: Dr. R. W. Drisko Port Hueneme, California 93401	1
Department of Physics & Chemistry Naval Postgraduate School Monterey, California 93940	1
Dr. A. L. Slafkosky Scientific Advisor Commandant of the Marine Corps (Code RD-1) Washington, D.C. 20380	1
Office of Naval Research Attn: Dr. Richard S. Miller 800 N. Quincy Street Arlington, Virginia 22217	1
Naval Ship Research and Development Center Attn: Dr. G. Bosmajian, Applied Chemistry Division Annapolis, Maryland 21401	1
Naval Ocean Systems Center Attn: Dr. S. Yamamoto, Marine Sciences Division San Diego, California 91232	1
Mr. John Boyle Materials Branch Naval Ship Engineering Center Philadelphia, Pennsylvania 19112	1

TECHNICAL REPORT DISTRIBUTION LIST, GEN

	No. Copies
Dr. Rudolph J. Marcus Office of Naval Research Scientific Liaison Group American Embassy APO San Francisco 96503	1
Mr. James Kelley DTNSRDC Code 2803 Annapolis, Maryland 21402	1

TECHNICAL REPORT DISTRIBUTION LIST, 359

	No. Copies
Dr. Paul Delahay Department of Chemistry New York University New York, New York 10003	1
Dr. E. Yeager Department of Chemistry Case Western Reserve University Cleveland, OH 44106	1
Dr. D. N. Bennion Chemical Engineering Department University of California Los Angeles, California 90024	1
Dr. R. A. Marcus Department of Chemistry California Institute of Technology Pasadena, California 91125	1
Dr. J. J. Auborn Bell Laboratories Murray Hill, New Jersey 07974	1
Dr. Adam Heller Bell Laboratories Murray Hill, New Jersey 07974	1
Dr. T. Katan Lockheed Missiles & Space Co, Inc. P.O. Box 504 Sunnyvale, California 94088	1
Dr. Joseph Singer, Code 302-1 NASA-Lewis 21000 Brookpark Road Cleveland, Ohio 44135	1
Dr. B. Brummer EIC Incorporated 55 Chapel Street Newton, Massachusetts 02158	1
Library P. R. Mallory and Company, Inc. Northwest Industrial Park Burlington, Massachusetts 01803	1
Dr. P. J. Hendra Department of Chemistry University of Southhampton Southhampton SO9 5NH United Kingdom	1
Dr. Sam Perone Department of Chemistry Purdue University West Lafayette, Indiana 47907	1
Dr. Royce W. Murray Department of Chemistry University of North Carolina Chapel Hill, North Carolina 27514	1
Naval Ocean Systems Center Attn: Technical Library San Diego, California 92152	1
Dr. C. E. Mueller The Electrochemistry Branch Materials Division, Research & Technology Department Naval Surface Weapons Center White Oak Laboratory Silver Spring, Maryland 20910	1
Dr. G. Goodman Globe-Union Incorporated 5757 North Green Bay Avenue Milwaukee, Wisconsin 53201	1
Dr. J. Boechler Electrochimica Corporation Attention: Technical Library 2485 Charleston Road Mountain View, California 94040	1
Dr. P. P. Schmidt Department of Chemistry Oakland University Rochester, Michigan 48063	1
Dr. H. Richtol Chemistry Department Rensselaer Polytechnic Institute Troy, New York 12181	1

TECHNICAL REPORT DISTRIBUTION LIST, 359

	No. Copies
Dr. A. B. Ellis Chemistry Department University of Wisconsin Madison, Wisconsin 53706	1
Dr. M. Wrighton Chemistry Department Massachusetts Institute of Technology Cambridge, Massachusetts 02139	1
Larry E. Plew Naval Weapons Support Center Code 30736, Building 2906 Crane, Indiana 47522	1
S. Ruby DOE (STOR) 600 E Street Washington, D.C. 20545	1
Dr. Aaron Wold Brown University Department of Chemistry Providence, Rhode Island 02192	1
Dr. R. C. Chudacek McGraw-Edison Company Edison Battery Division Post Office Box 28 Bloomfield, New Jersey 07003	1
Dr. A. J. Bard University of Texas Department of Chemistry Austin, Texas 78712	1
Dr. M. M. Nicholson Electronics Research Center Rockwell International 3370 Miraloma Avenue Anaheim, California	1
Dr. Donald W. Ernst Naval Surface Weapons Center Code R-33 White Oak Laboratory Silver Spring, Maryland 20910	1
Dr. R. P. Van Duyne Department of Chemistry Northwestern University Evanston, Illinois 60201	1
Dr. B. Stanley Pons Department of Chemistry Oakland University Rochester, Michigan 48063	1
Dr. Michael J. Weaver Department of Chemistry Michigan State University East Lansing, Michigan 48824	1
Dr. R. David Rauh EIC Corporation 55 Chapel Street Newton, Massachusetts 02158	1
Dr. J. David Margerum Research Laboratories Division Hughes Aircraft Company 3011 Malibu Canyon Road Malibu, California 90265	1
Dr. Martin Fleischmann Department of Chemistry University of Southampton Southampton 509 5NH England	1
Dr. Janet Osteryoung Department of Chemistry State University of New York at Buffalo Buffalo, New York 14214	1
Dr. R. A. Osteryoung Department of Chemistry State University of New York at Buffalo Buffalo, New York 14214	
Mr. James R. Moden Naval Underwater Systems Center Code 3632 Newport, Rhode Island 02840	

TECHNICAL REPORT DISTRIBUTION LIST, 359

	No. Copies
Dr. R. Nowak Naval Research Laboratory Code 6130 Washington, D.C. 20375	1
Dr. John F. Houlihan Shenango Valley Campus Penn. State University Sharon, PA 16146	1